

This is to certify that the

thesis entitled

Adsorption and Photochemistry of 1,3-Butadiene on HOPG(0001)

presented by

Jason K. Oman

has been accepted towards fulfillment of the requirements for

M.S. degree in Chemistry

Date 4/15/02

MSU is an Affirmative Action/Equal Opportunity Institution

O-7639

LIBRARY Michigan State University

PLACE IN RETURN BOX to remove this checkout from your record.

TO AVOID FINES return on or before date due.

MAY BE RECALLED with earlier due date if requested.

DATE DUE	DATE DUE	DATE DUE
,		
	<u> </u>	

6/01 c:/CIRC/DateDue.p65-p.15

ADSORPTION AND PHOTOCHEMISTRY OF 1,3-BUTADIENE ON HOPG (0001)

Ву

Jason Kenneth Oman

A THESIS

Submitted to
Michigan State University
in partial fulfillment of the requirements
for the degree of

MASTER OF SCIENCE

Department of Chemistry

2002

ABSTRACT

ADSORPTION AND PHOTOCHEMISTRY OF 1,3-BUTADIENE ON HOPG(0001)

By

JASON KENNETH OMAN

The adsorption and photochemistry of 1,3-butadiene (C_4H_6) on HOPG(0001) at < 85 K was studied using temperature-programmed desorption (TPD) and electron energy loss spectroscopy (EELS). Butadiene weakly adsorbs on HOPG, the monolayer (ML) exhibiting first order desorption with a maximum desorption rate at 129 K and a corresponding desorption energy of 32 kJ/mol. Multilayer butadiene showed zero order desorption with a maximum desorption rate at 105 K and a desorption energy of 28.5 kJ/mol. Irradiation of the C₄H₆/HOPG(0001) surface (1 and 3 monolayers of C₄H₆) with UV photons (193 nm, 248 nm, and 351 nm) at 100 mJ/pulse resulted in molecular photodesorption of the adsorbed butadiene layers. The cross section for photodesorption was calculated at each wavelength for both coverages. For 1 monolayer coverage, the cross-sections were 3.3×10^{-20} cm², 2.4×10^{-20} cm², and 1.2×10^{-20} cm² for 193 nm, 248 nm, and 351 nm, respectively. The 3 monolayer cross-sections were 1.1×10^{-17} cm², 6.3×10^{-18} cm², and 1.8x10⁻¹⁸ cm² for 193 nm, 248 nm, and 351 nm, respectively. It was found the photodesorption mechanism could be described by a simple thermal process. The photoprocesses occurring in both 1 and 3 ML C₄H₆(ad)/HOPG were also investigated at lower photon fluences of ≤ 10 mJ/pulse. Under these conditions, there was no detectable photodesorption or condensed phase photochemistry.

ACKNOWLEDGMENTS

I would like to thank everyone who was involved with my work at MSU. Especially Dr. Simon Garrett for his guidance, support and I'm sure at times patience. I would also like to thank all the group members (Todd, Lilli, Mike and Heather), and I can't forget the new group members Anne and Steve. They have all been helpful with my research and provided a break from work every now and again.

I would also like to thank my family and friends for without their support during the course of this work it would not have been accomplished, (mom, dad, Debi, Andrew, Matt, Dave and Eric). I would also like to give Melissa a special thanks for having to put-up with me during the most stressful times here at MSU.

TABLE OF CONTENTS

		Page
LIST (OF TABLES	vi
LIST (OF FIGURES	vii
INTRO	DDUCTION	1
1.1	Heterogeneous Atmospheric Chemistry	1
1.2	Atmospheric Photochemistry	5
1.3	Carbonaceous Particles in the Atmosphere	6
1.4	Unsaturated Hydrocarbons in the Atmosphere	9
1.5	Proposed System	10
1.6	References	17
EXPE	RIMENTAL	20
2.1	Survey of Analytical Techniques	20
2.2	Experimental Apparatus	25
2.3	References	30
ADSC	RPTION AND PHOTOCHEMISTRY OF 1,3-BUTADIENE ON HOPG	31
3.1	Adsorption of Butadiene on HOPG determined by TPD	31
3.2	Adsorption of Butadiene on HOPG determined by EELS	33
3.3	Photodesorption of Butadiene monitored by TPD	38
3.4	Photodesorption of Butadiene monitored by EELS	43
DISC	JSSION	45
3.5	Mechanisms for Photodesorption	45
3.6	Adsorbate-mediated Processes	45
3.7	Substrate-mediated Processes	46
3.8	Laser-induced Thermal Desorption	47
3.9	Conclusions	52
CONC	CLUSIONS AND FUTURE WORK	56
4.1	Adsorption and Photochemistry of Butadiene on HOPG	56

4.2	Future work	57
4.3	References	63
APPE	NDICES	64
App	endix A Mass Spectra	65
App	endix B Calculation of Desorption Energies for Butadiene on HOPG	67
Appe	endix C Calculation for energy absorbed by HOPG during laser irradiation	68
Refe	rences	69

LIST OF TABLES

		Page
Table 3.1	Vibrational assignments of 1,3-Butadiene adsorbed on HOPG(0001).	37
Table 3.2	Butadiene photodesorption cross sections and gas phase cross sections from the literature.	41

LIST OF FIGURES

		Page
Figure 1.1	Variation of temperature and pressure from ground level to 100 km above the Earth's surface.	2
Figure 1.2	Surface catalyzed heterogeneous reaction between chlorine nitrate and a polar stratospheric cloud particle (PSC).	4
Figure 1.3	Comparison of the solar spectrum outside the atmosphere, a 5800 K blackbody radiator and the solar spectrum at sea level.	7
Figure 1.4	General oxidation sequence for hydrocarbons and organic molecules in the atmosphere.	11
Figure 1.5	Single-bond rotation isomerization of 1,3-butadiene.	13
Figure 1.6	Graphite crystal structure showing basal plane dimension and bond lengths.	16
Figure 2.1	Schematic diagram of X-ray photoelectron generation.	21
Figure 2.2	Representation of a dipole perpendicular to a surface and its image dipole in the surface (left) and a dipole parallel to a surface plane with its mirror image in the surface (right).	24
Figure 2.3	X-ray photoelectron spectrum of the HOPG surface before experiments.	27
Figure 2.4	Experimental apparatus showing excimer laser and UHV chamber orientation.	28

		Page
Figure 3.1	Mass (C ₃ H ₃ ⁺) thermal desorption spectra of C ₄ H ₆ on HOPG with increasing coverage. At 2.0 ML coverage the 1st monolayer saturates.	32
Figure 3.2	Thermal desorption spectra for masses 39 ($C_3H_3^+$), 27 ($C_2H_3^+$) and 54 ($C_4H_6^+$) of C_4H_6 on HOPG for \leq 3 ML coverage to ensure the 1st monolayer is saturated.	34
Figure 3.3	Electron energy loss spectra of (a) 1 ML and (b) 3 ML C ₄ H ₆ on HOPG.	36
Figure 3.4	Thermal desorption spectra (mass 39, $C_3H_3^+$) of 1 ML C_4H_6 on HOPG irradiated with increasing photon number ($\lambda = 193$ nm).	39
Figure 3.5	Thermal desorption spectra (mass 39, $C_3H_3^+$) of 3 ML C_4H_6 on HOPG irradiated with increasing photon number ($\lambda = 193$ nm).	40
Figure 3.6	Semi-logarithmic plot of TPD peak area vs. total number of photons/cm ² for calculation of the photodesorption cross section.	42
Figure 3.7	Electron energy loss spectra of 3 ML C ₄ H ₆ on HOPG exposed to 1x10 ¹⁷ photons/cm ² .	44
Figure 3.8	Result for calculating the surface temperature rise using equation 1 when HOPG is exposed to a 16 ns 100 mJ pulse of 193 nm light.	50

		Page
Figure 3.9	Percent of C_4H_6 monolayer desorbed from the surface with increasing pulse power. The total number of photons was kept constant at each pulse power by varying the number of pulses.	51
Figure 4.1	Temperature programmed desorption spectra (mass 94) for CH ₃ Br on HOPG with increasing exposure time; a) 1 sec, b) 5 sec, c) 10 sec, d) 20 sec, e) 40 sec, f) 60 sec.	59
Figure 4.2	X-ray photoelectron spectra of 1 ML CH ₃ Br exposed to 5 mJ/pulses at 10 Hz of 193 nm light for increasing times; a) 30 min, b) 10 min, c) 5 min, d) 2.5 min, e) 0.5 min, f) 0 min showing binding energy changes.	60
Figure A.1	Mass spectra of (a) 1,3-butadiene at a pressure of 5×10^{-9} Torr and (b) the background vacuum of the UHV chamber at a pressure of 2 x 10^{-10} Torr.	66

INTRODUCTION

1.1 Heterogeneous Atmospheric Chemistry

The atmosphere is a layer of gas that surrounds the Earth and contains molecules necessary for respiration, helps regulate temperature and climate on the Earth's surface and acts as a sink for gases and particles produced from biological activity, combustion processes and anthropogenic sources. Temperature and pressure both vary throughout the atmosphere; Figure 1.1 shows a vertical profile from 0 to 100 km above the Earth's surface. Notice, the atmosphere is divided into several separate layers which are described based on temperature gradients. The troposphere, closest to the Earth's surface, contains 80% of all atmospheric mass and the majority of all atmospheric species, both molecular and particulate. Above the troposphere is the stratosphere; this layer of the atmosphere contains a high concentration of ozone (up to 10 ppm) which filters UV radiation preventing it from reaching the Earth's surface. The mesosphere and thermosphere are high-altitude layers of the atmosphere containing few molecular species and are characterized by low pressures.

Over the past few decades, heterogeneous reactions on solid particle or aerosol surfaces have been found to play an important role in atmospheric chemistry. Examples of aerosol particles include liquid water, ice, sea-salt, metal oxides, aluminosilicates and carbonaceous matter or mixtures of some of these species. A majority of the research conducted to date has focused on heterogeneous reactions on model polar stratospheric cloud surfaces (PSCs) that contribute to ozone destruction. For example, the reaction between ice or nitric acid-

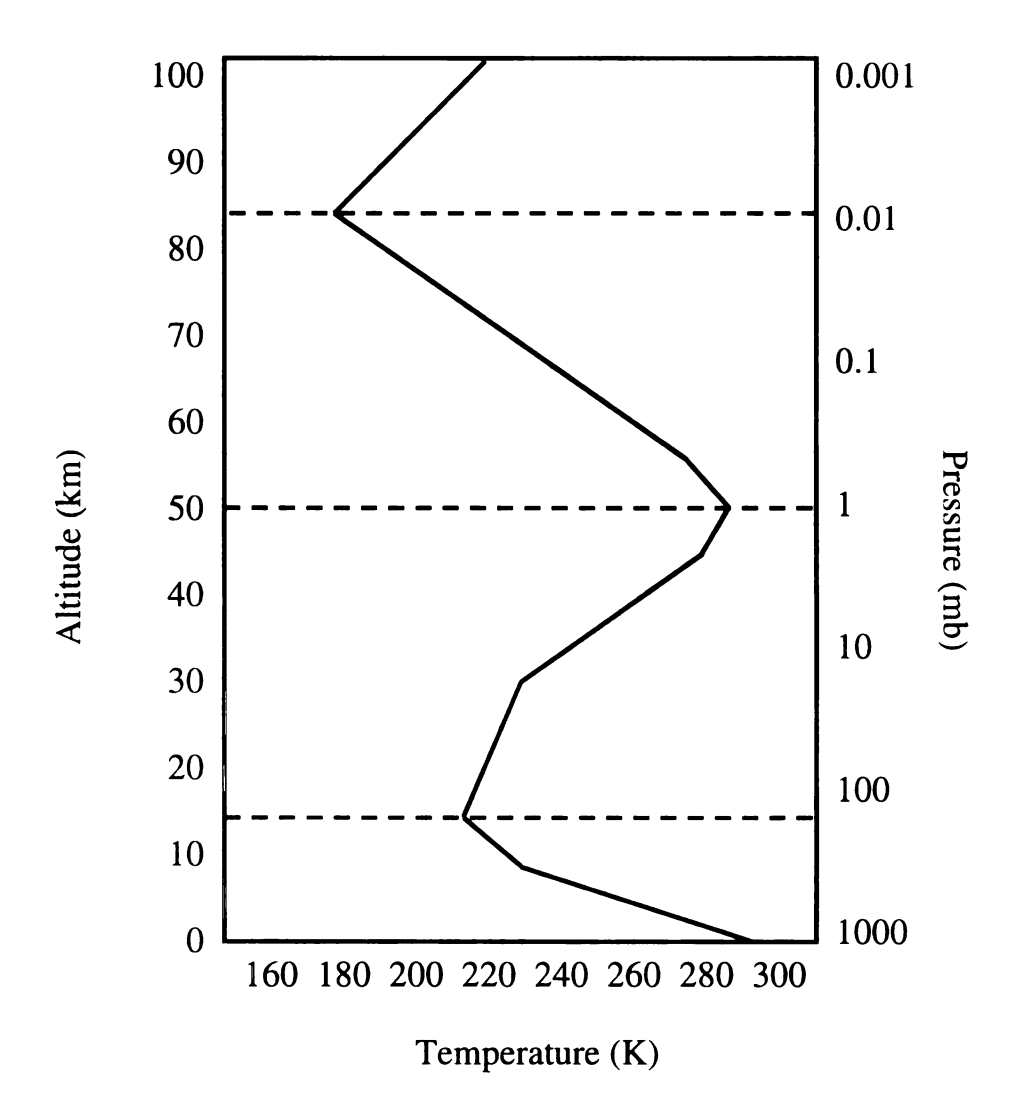


Figure 1.1 Variation of temperature and pressure from ground level to 100 km above the Earth's surface. I

containing ice and chlorine nitrate molecules produces molecular chlorine that is liberated from the ice surface.⁵ Molecular chlorine is photolyzed by sunlight (λ < 380 nm) to produce free chlorine atoms that subsequently participate in reactions destroying ozone (see Figure 1.2). The formation of the ozone hole is a yearly event; surfaces that catalyze reactions producing photo-destructive molecules are only present during the winter months. During spring/summer the ozone-depleting species react in the gas phase to reform photoinactive molecules that do not contribute to ozone destruction.

The impact heterogeneous reactions have on atmospheric chemistry may be much greater than previously realized. One reason for this misconception is a relatively small portion of atmospheric mass is condensed matter ($< 2 \times 10^{-6} \%$). However, surfaces contain active sites which catalyze reactions that would never be considered to be important in the gas phase. Unfortunately, the composition and concentration of particulate matter varies greatly in both time and space in the atmosphere making heterogeneous reactions in the atmosphere difficult to predict and model. Understanding how particulate matter impacts chemistry in the atmosphere and the reactions that these surfaces catalyze is crucial for understanding the dynamics of the atmosphere.

Heterogeneous chemistry of NO₂ and H₂O on soot or carbon black particles has been shown to play an important role in tropospheric chemistry.⁶ Carbonaceous aerosols reduce NO₂ in the presence of H₂O to produce HONO. It has been shown that the gas phase reaction between NO₂ and H₂O is too slow to produce significant amounts of HONO under atmospheric conditions.⁷ The heterogeneous production of HONO on carbonaceous particles is fast enough to account for the high night-time levels of

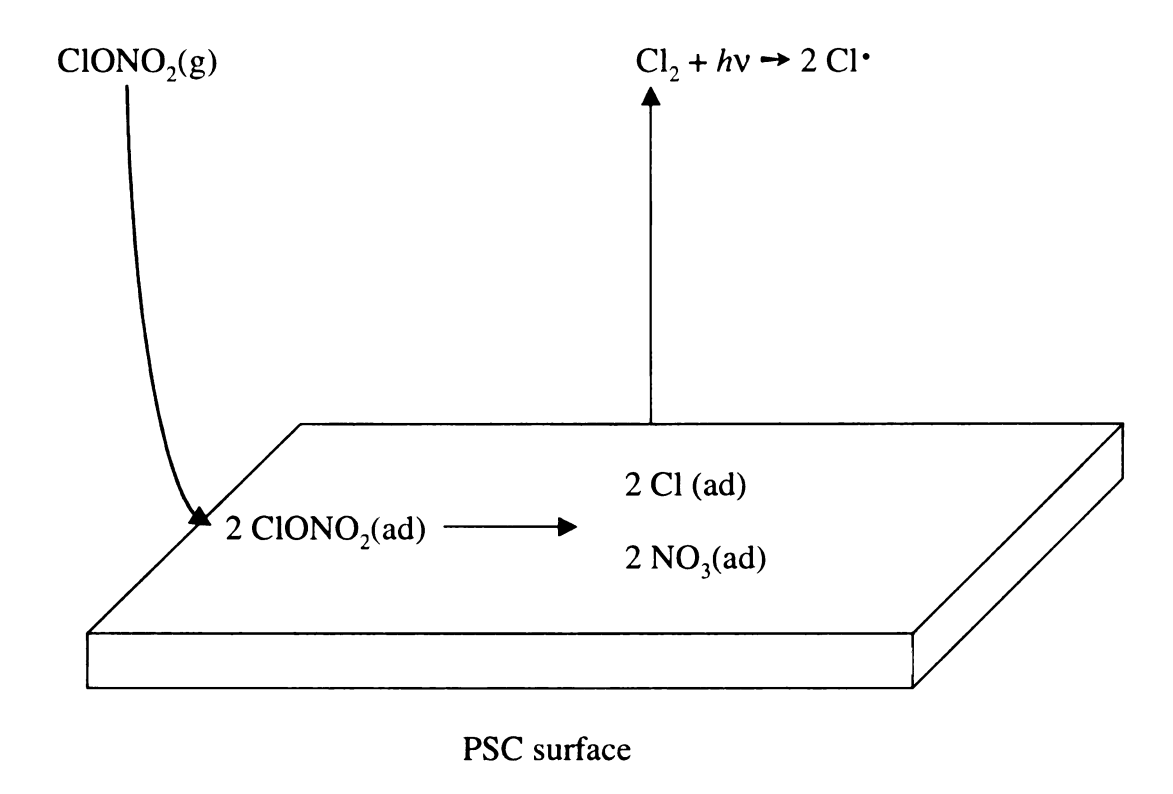


Figure 1.2 Surface catalyzed heterogeneous reaction between chlorine nitrate and a polar stratospheric cloud particle (PSC).⁵

HONO.⁷ This reaction is important because HONO is readily photolyzed in the troposphere by sunlight at wavelengths between 380 and 330 nm⁸ to produce ·OH and NO·. The ·OH and NO· produced then participate in a series of important gas phase reactions such as the production of O₃ and the initial oxidation steps of organic molecules in the troposphere.

1.2 Atmospheric Photochemistry

Much of the chemistry that takes place in the atmosphere is known to be the result of photochemical processes. The sun behaves similar to a blackbody radiator emitting a broad range of wavelengths ($\lambda = 100 \text{ nm}$ to 1000 nm) that penetrate the Earth's atmosphere. This range of wavelengths enters the atmosphere and interacts with molecules inducing a variety of photochemical processes. Ultraviolet and visible light is of sufficient energy to excite electronic transitions in many molecular or atomic species. When a molecule absorbs a photon of light it undergoes an electronic transition to an excited state. The energy between the excited state and the ground state is equal to the energy of the photon that was absorbed. Different atomic and molecular species absorb different wavelengths based upon energy differences between their initial and final electronic states. Once in the excited state, a molecule can undergo several different processes to lose the absorbed energy, including reemission of a photon via fluorescence, transfer of energy through collisions with other molecules (called quenching), chemical reaction with another molecule to produce a new species, or dissociation into two (or more) species (called photolysis).

Absorption of radiation resulting in photodissociation is very common in the atmosphere and an important mechanism for preventing high-energy radiation from reaching the Earth's

surface where it can harm organisms. Figure 1.3 compares the differences in the solar spectrum outside the atmosphere and at sea level. The reduction of total flux at sea level is due to the absorption of radiation by atmospheric species in the ultraviolet, visible and infrared regions of the solar spectrum.⁹ In the upper atmosphere (175 km-80 km) molecules such as oxygen and nitrogen are the main species that absorb and filter out high-energy radiation ($\lambda < 175$ nm).¹⁰ Another species that filters out UV radiation ($\lambda = 210$ nm-300 nm)¹⁰ is ozone found in the stratosphere (15 km-50 km). Wavelengths > 300 nm can reach both the troposphere and the Earth's surface. Solar flux of wavelengths > 300 nm into the troposphere is on the order of 1×10^{14} photons cm⁻² sec⁻¹. ¹

1.3 Carbonaceous Particles in the Atmosphere

Recent interest has focused on the atmospheric chemistry of carbonaceous or organic aerosols^{2,7,11} since a significant fraction (up to 30% in urban areas)¹ of all atmospheric particulate matter is carbonaceous.¹² The composition of organic aerosol particles within the atmosphere shows large spatial and temporal variations. The formation and exact composition of these particles is complex, difficult to measure and not well understood,^{13,14} but they can include condensed biogenic organic molecules, soot, and polycyclic aromatic hydrocarbons (PAHs). Incomplete combustion processes, such as the burning of fossil fuels or biomass, are the major anthropogenic sources of the latter two types of carbonaceous particles in the atmosphere.¹⁵ Penner and Novakov define soot as consisting of a soluble organic fraction and an insoluble component that is resistant to oxidation.¹⁵ The insoluble component has been variously termed elemental, graphitic or black carbon. There is some evidence that this component contains a

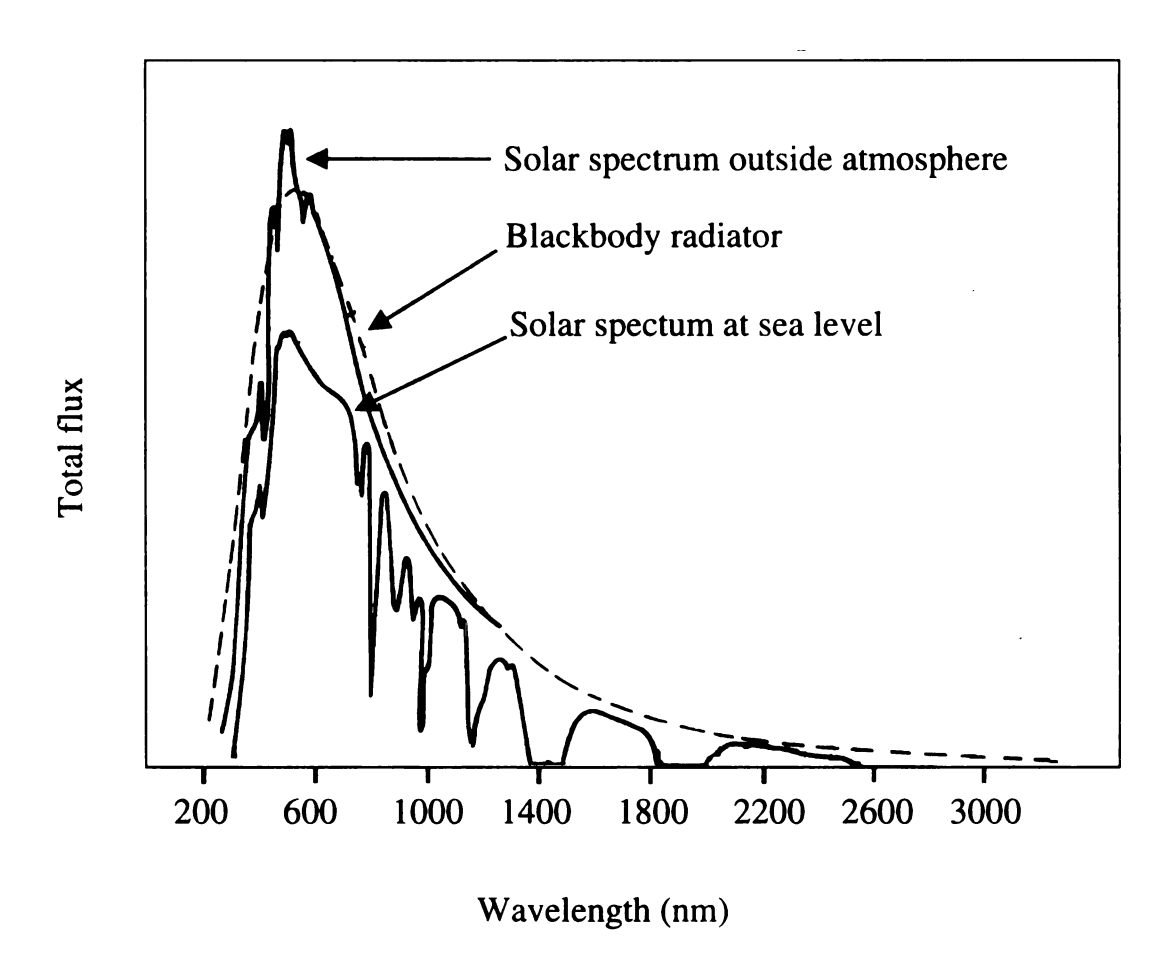


Figure 1.3 Comparison of the solar spectrum outside the atmosphere, a 5800 K blackbody radiator and the solar spectrum at sea level. 10

graphite-like microcrystalline structure. ¹⁶ Black carbon particles can act as condensation nuclei and as sites for heterogeneous reactions in the atmosphere. Indeed, it has been speculated that fast reactions on black carbon surfaces could strongly affect atmospheric chemistry. ¹⁵

The residence time of carbonaceous aerosols in the atmosphere is highly size-dependant. Particles with a diameter of about 1 μ m have a long residence time, about 1×10^6 sec at 1.5 km. Residence time decreases for particles that are either larger or smaller than 1 μ m. For example, particles $\cong 0.001$ μ m or $\cong 10$ μ m have residence times of about 100 sec at an altitude of 1.5 km. Small particles, diameter ≤ 0.001 μ m are typically removed through nucleation processes by sticking to larger particles in the troposphere. Large aerosols, with diameters ≥ 10 μ m, undergo gravitational settling. Intermediate size particles, about 1 μ m in diameter, are not significantly affected by either deposition route and therefore have long residence times in the atmosphere.

Atmospheric aerosol surfaces can be labeled as being either rigid or dynamic.⁷ A surface is considered to be dynamic when the vapor phase of the solid condenses on to the surface at a high rate. This provides a consistently refreshed surface for any heterogeneous reactions that are catalyzed by the surface. The surface of a rigid solid is not refreshed regularly by a high condensation flux. A catalytically active rigid surface can be permanently changed or altered by a reacting species; (this process is analogous to the poisoning of an electrode surface). Of course, poisoning of the surface from one reaction may allow the modified surface to catalyze another reaction. Graphitic or carbon black aerosols are considered to be rigid solids.⁷

A typical young carbon black particle has a C/H ratio of ~3-4¹³ and the particle surface at this point is considered to be hydrophobic, preferentially adsorbing hydrocarbon vapor over water vapor.⁷ The preference for hydrocarbon adsorption on graphitic surfaces may play an important role in the heterogeneous chemistry of organic molecules. Carbonaceous particles are susceptible to the formation of functional groups on the surface.⁷ Typical functional groups are oxidation products such as mono or dicarboxylic acids or C=O.¹⁴ The addition of oxygen-containing functional groups to the carbon surface makes the surface more polar.

1.4 Unsaturated Hydrocarbons in the Atmosphere

Unsaturated organic molecules enter the atmosphere through a variety of pathways including combustion of fossil fuels and biomass, industrial processes and biogenic releases. Biogenic sources (mainly plants) release significant amounts of unsaturated organics including isoprene (2-methyl-1,3-butadiene) and monoterpenes. The yield of these releases is estimated to be 1x10¹² kg/yr. Rorest fires are also known to release a broad range of unsaturated molecular species to the atmosphere. One particular study has shown an extensive list (about 20 species) of unsaturated molecules present in North American forest fire plumes, including ethene, propene, 1,3-butadiene, pentene, isoprene and octene. 19 1,3-Butadiene is an example of an unsaturated organic molecule that is commonly found in the atmosphere from several major sources including automobile exhaust, forest fires and industrial processes. It is estimated that, in California, local automobile exhaust contributes to about 96% of the annual emissions of 1,3-butadiene to

the troposphere. The average daytime concentration of butadiene measured in Los Angeles is 2.2 ppb.²⁰

Once in the atmosphere, unsaturated molecules undergo numerous oxidation reactions, many ultimately leading to the final products CO₂ and H₂O. ¹ Strong atmospheric oxidizers such as hydroxyl radicals, nitrate radicals, ozone and molecular chlorine initiate the oxidation of unsaturated molecules. A wide range of reactive intermediates, including organic peroxy radicals, organic nitrates, alkoxy radicals, aldehydes, ketones, alcohols and organic acids may be formed. Figure 1.4 shows a general outline of oxidation processes organic molecules undergo in the atmosphere. For example, in one study, gas-phase butadiene was exposed to hydroxyl radicals and/or nitrate radicals and nitric oxide, ²⁰ and the major products were found to be acrolein, HCHO, furan and numerous organic nitrate isomers. A broad range of gas phase chemical reactions are known to take place in the atmosphere, but it is still unclear what role the surfaces of carbonaceous and other aerosols may play in catalyzing these reactions.

1.5 Proposed System

Our laboratory is interested in investigating adsorption and photochemistry of small atmospherically relevant organic molecules on carbonaceous surfaces, using graphite as a model for carbonaceous particulate matter. In this thesis, an initial study of the adsorption and photochemistry of 1,3-butadiene on graphite is presented. Experiments were conducted under ultrahigh vacuum (UHV) conditions, (pressure ~1.7x10⁻¹⁰ torr). The photochemistry was initiated with ultraviolet (193, 248 and 351 nm) photons generated by an excimer laser. Analytical techniques used to study this system included

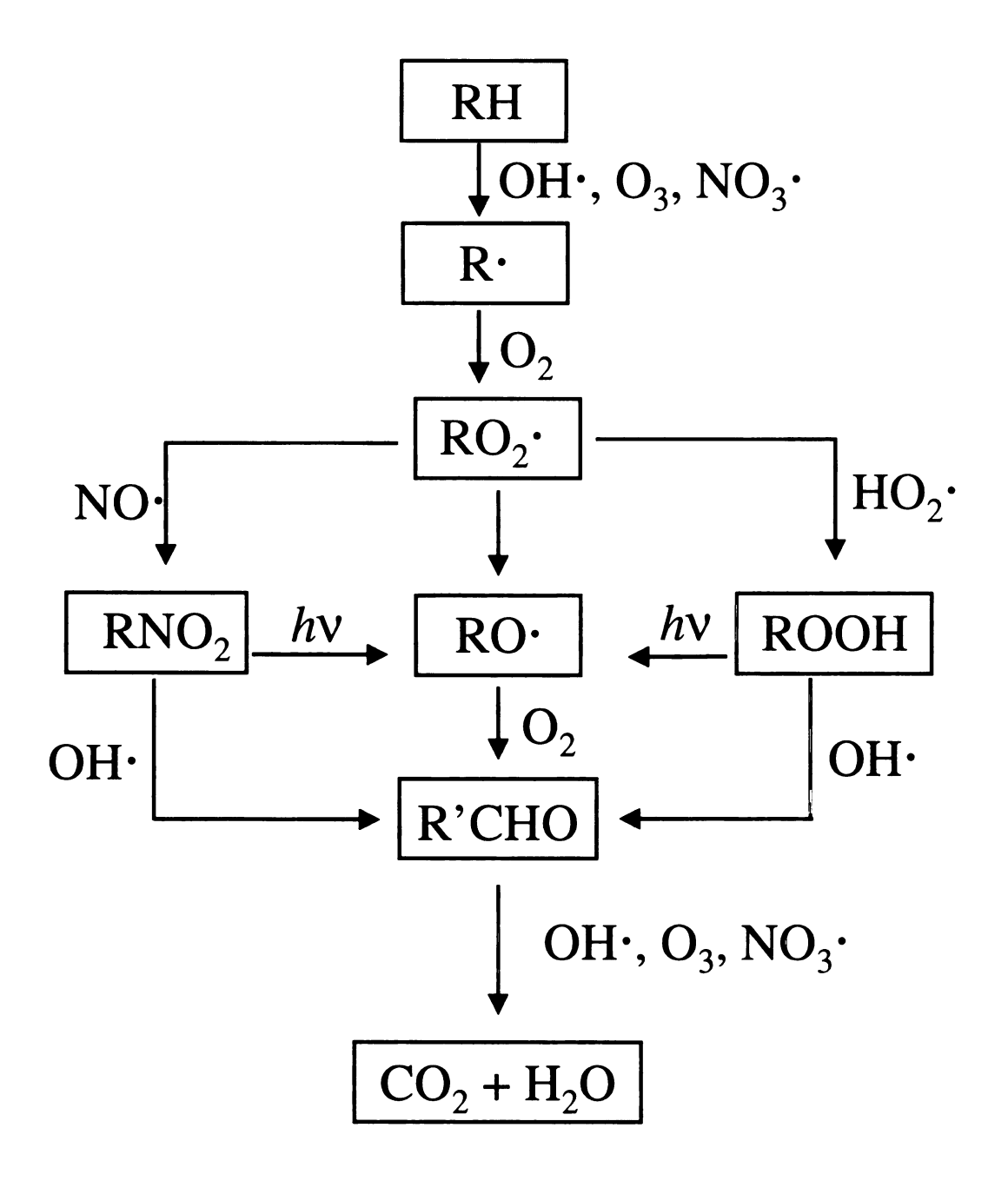


Figure 1.4 General oxidation sequence for hydrocarbons and organic molecules in the atmosphere.¹

temperature programmed desorption (TPD) and high resolution electron energy loss spectroscopy (HREELS). The goal of this work was to identify the adsorption structure of butadiene on the graphite surface, and characterize any photochemistry that may take place at the butadiene/graphite interface.

1,3-Butadiene was chosen both because it is environmentally relevant and its gas phase chemistry has been well studied. It is the simplest conjugated molecule, consisting of 4 carbon atoms that are sp^2 hybridized resulting in a short enough bond length between C2 and C3 for their p orbitals to somewhat overlap. Overlap between C2 and C3 gives the central bond partial double bond character to allow for delocalization of all 4 π electrons over all of the 4 carbon atoms. Delocalized bonding of this nature increases the stability of the molecule.^{21,22} In theory, butadiene can form three different structural isomers by rotation around C2 and C3, these are labeled s-trans, s-cis and gauche. Note, the s preceding trans and cis designations refers to isomers formed by rotation around a single bond.²¹ The *trans* isomer, with C_{2h} symmetry, is the thermodynamically most stable and at room temperature > 99% of the molecules will take on this conformation.²³ The *cis* conformer, with C_{2v} symmetry, is thought to be the second most stable conformation of butadiene, and is formed by a 180° rotation around the C2-C3 bond as shown in Figure 1.5. The cis (planar or almost planar) isomer is also stabilized by delocalized π bonding across all four carbon atoms but unfavorable van der Walls interactions between hydrogens on C1 and C4 destabilizes the molecule relative to the trans isomer by about 12 kJ/mol.²¹ The intermediate between the trans and cis isomers is a gauche structure. In the gauche conformation, p orbitals between C2 and C3 will be perpendicular to each other, preventing delocalized π bonding throughout the system.

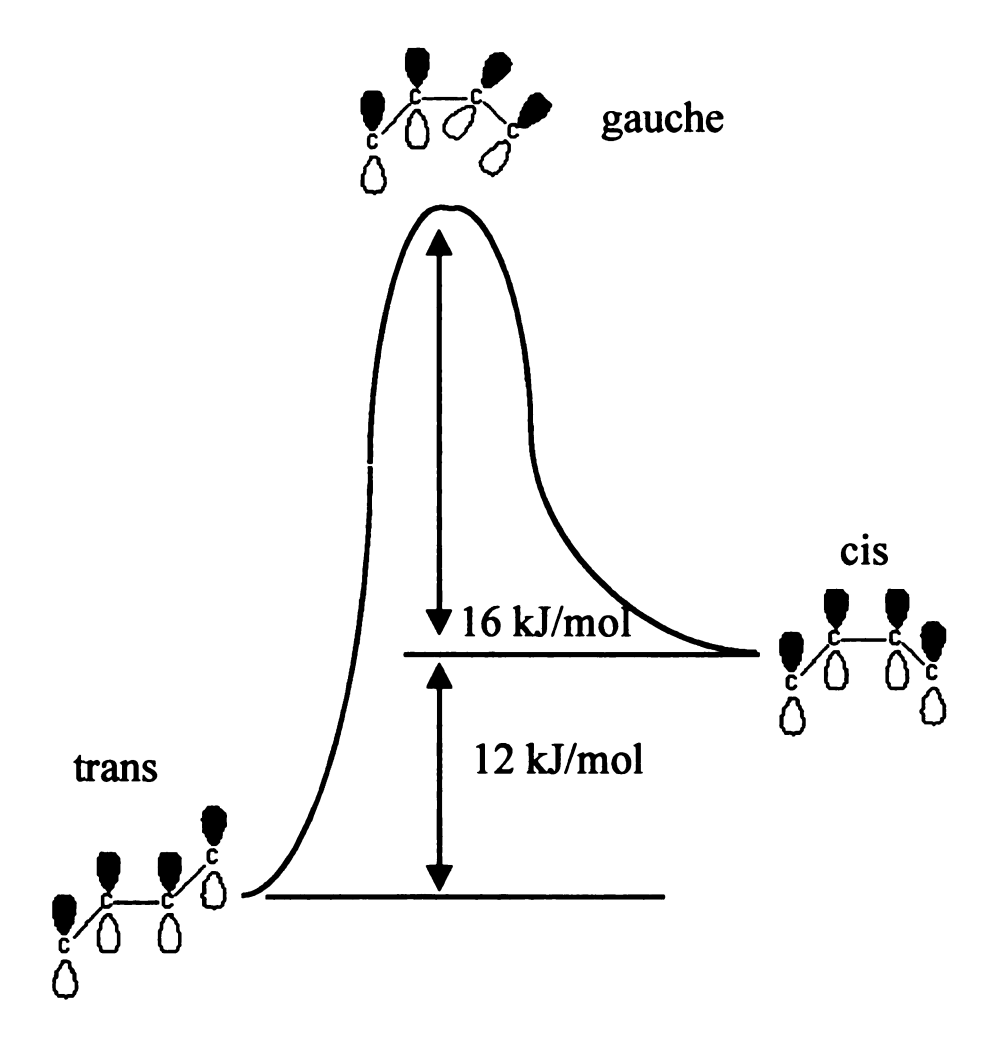


Figure 1.5 Single-bond rotation isomerization of 1,3-butadiene.²¹

This decreases the stability of the *gauche* isomer by about 28 kJ/mol relative to the *trans* conformer.²¹

Gas-phase butadiene absorbs UV radiation from about 170 nm to 225 nm.²⁴ The wavelength of maximum absorption is 210 nm, where the absorption cross section is $1x10^{-16}$ cm².²⁵ In this wavelength range, absorption results in a $\pi \rightarrow \pi^*$ transition to two closely spaced states (the 1B_u and 2A_g states). These states have short lifetimes of <100 fs, and decay from these states eventually leads to single-bond isomerization in about 270 fs.²⁶ Haller *et al.* studied the photolysis of butadiene both in the gas phase and in a cyclohexane solution.²⁷ At low pressure, (4 mm Hg) the gas phase photolysis of butadiene using wavelengths between 200 nm and 280 nm produced a series of products such as hydrogen, acetylene, ethene, ethane, 1-butyne and 1,2-butadiene.²⁷ It is thought a vibrationally excited state is the precursor to the products. In the same experiment butadiene was also found to polymerize on the walls of the vacuum chamber. In solution the major products were found to be cyclobutene and bicyclobutane.²⁷

Several ultrahigh vacuum studies have been published identifying adsorption structures of butadiene on single metal crystals. $^{28-32}$ The catalytic behavior of metal surfaces toward selective hydrogenation of dienes and other unsaturated organic molecules has spurred much of this work. Some of the most interesting work by Bertolini *et al.* compared the chemistry of butadiene on Pt(111) and Pd(111). 28 On Pt(111), the π bonds of butadiene are activated to produce a di- σ metallacycle species where half the carbon atoms in the butadiene molecule rehybridize from sp^2 to sp^3 . Butadiene maintains its hybridization on the Pd(111) surface and forms a di- π bonded species. Butadiene adsorption has also been studied on more inert surfaces, such as

Au(111) and Ag(111), where adsorbate/surface interactions are presumed to be weak.³² Based on inferred reflection-absorption spectroscopy, Osaka *et al.* suggests butadiene adsorbs on Au(111) with its π bonds parallel to the surface in the *trans* conformation.

Highly ordered pyrolytic graphite (HOPG or graphite) will be used as a model for carbonaceous aerosol surfaces. Highly ordered pyrolytic graphite is produced when pyrolytic graphite is annealed at temperatures of 3000 °C. 33 The crystal structure of graphite, shown in Figure 1.6, is composed of layered basal planes, 33 the distance between planes being 3.35 Å. 34 Each basal plane of graphite is composed of fused hexagons containing sp^2 hybridized carbon atoms with C-C bond lengths of 1.4 Å. 34 Graphite is a semimetal with a workfunction of 4.4 eV. 35

As previously mentioned, the structure of the basal plane of graphite is similar to the microcrystalline component of soot or carbon black. This component is resistant to oxidation and insoluble in most organic solvents. Carbon atoms in the microcrystalline component of carbonaceous aerosols are sp^2 hybridized with carbon-carbon bond lengths similar to that of graphite. The basis for using graphite as a model for carbonaceous aerosols stems from the structural similarities between the two species. As such, the graphite surface is a starting point for investigating heterogeneous photochemistry that is relevant to atmospheric reactions on carbonaceous aerosols.

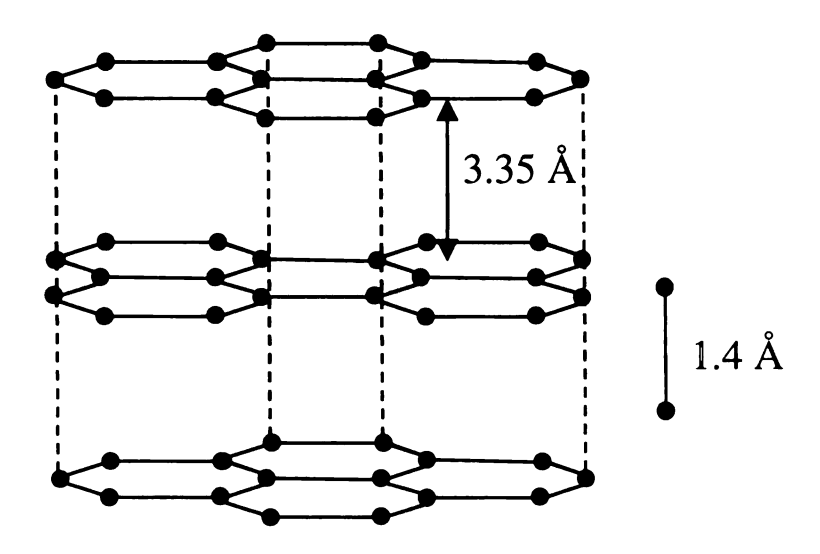


Figure 1.6 Graphite crystal structure showing basal plane dimension and bond lengths.³³

1.6 References

- (1) Brasseur, G. P.; Orlando, J. J.; Tyndall, G. S. *Atmospheric Chemistry and Global Change*; Oxford University Press, Inc. New York, 1999.
- (2) Grassian, V. H. Int. Rev. Phys. Chem. 2001, 20, 467.
- (3) Zondlo, M. A.; Hudson, P. K.; Prenni, A. J.; Tolbert, M. A. *Annu. Rev. Phys. Chem.* 2000, *51*, 473.
- (4) Peter, T. Annu. Rev. Phys. Chem. 1997, 48, 785.
- (5) Zondlo, M. A.; Barone, S. B.; Tolbert, M. A. J. Phys. Chem. A 1998, 102, 5735.
- (6) Ammann, M.; Kalberer, M.; Jost, D. T.; Tobler, L.; Rossler, E.; Piguet, D.; Gaggeler, H. W.; Baltensperger, U. *Nature* 1998, 395, 157.
- (7) Ravishankara, A. R.; Longfellow, C. A. Phys. Chem. Chem. Phys. 1999, 1, 5433.
- (8) Grassian, V. H. J. Phys. Chem. A 2002, 106, 860.
- (9) Parmon, V. N.; Zakharenko, V. S. *Cattech* 2001, 5, 96.
- (10) Finlayson-Pitts, B. J.; James N. Pitts, J. Chemistry of the Upper and Lower Atmosphere; Academic Press: New York, 2000.
- (11) Pandis, S. N.; Wexler, A. S.; Seinfield, J. H. J. Phys. Chem. 1995, 99, 9646.
- (12) Andreae, M. O.; Crutzen, P. J. Science 1997, 276, 1052.
- (13) Homann, K.-H. Angew. Chem. Int. Ed. 1998, 37, 2434.
- (14) Lary, D. J.; Shallcross, D. E.; Toumi, R. J. Geophys. Res. 1999, 104, 15929.
- (15) Penner, J. E.; Novakov, T. J. Geophys. Res. 1996, 101, 19373.
- (16) Rosen, H. *Nature* T. Novakov, 266, 708.
- (17) Graedel, T. E.; Crutzen, P. J. Atmospheric Change An Earth System Perspective; W. H. Freeman and Company: New York, 1993.

- (18) Atkinson, R.; Arey, J. Acc. Chem. Res. 1998, 31, 574.
- (19) Friedli, H. R.; Atlas, E.; Stroud, V. R.; Giovanni, L.; Campos, T.; Radke, L. F. *Global Biogeochemical Cycles* 2001, *15*, 435.
- (20) Tuazon, E. C.; Alvardo, A.; Aschmann, S. M.; Atkinson, R.; Arey, F. Environ. Sci. Technol. 1999, 33, 3586.
- (21) Carey, F. A. Organic Chemistry, 2nd ed.; McGraw-Hill, Inc: New York, 1992.
- (22) Traven, V. F. Frontier Orbitals and Properties of Organic Molecules; Ellis Horwood: New York, 1992.
- (23) Wiberg, K. B.; Rosenberg, R. E. J. Am. Chem. Soc. 1990, 112, 1509.
- (24) Calvert, J. G.; Pitts Jr., J. N. *Photochemistry*; John Wiley and Sons: New York, 1966.
- (25) Fahr, A.; Nayak, A. K. Chem. Phys. 1994, 189, 725.
- (26) Fub, W.; Schmid, W. E.; Trushin, S. A. Chem. Phys. Lett. 2001, 342, 91.
- (27) Haller, I.; Srinivasan, R. J. Chem. Phys. 1964, 40, 1992.
- (28) Bertolini, J. C.; Cassuto, A.; Jugnet, Y.; Massardier, J.; Tardy, B.; Tourillon, G. Surf. Sci. 1996, 349, 88.
- (29) Bhattacharya, A. K.; Pyke, D. R. J. Mol Cat. A 1998, 129, 279.
- (30) Chen, J. G. J. Catal. A 1995, 154, 80.
- (31) Weiss, M. J.; Hagedorn, C. J.; Weinberg, W. H. J. Vac. Sci. Technol. A 2000, 18, 1443.
- (32) Osaka, N.; Akita, M.; Itoh, K. J. Phys. Chem. B 1998, 102, 6817.
- (33) Borghesi, A.; Guizzetti, G. *Handbook of Optical Constants of Solids 2*; Academic Press: New York, 1991.

- (34) Reynolds, W. N. *Physical Properties of Graphite*; Elsevier Publishing Co.: New York, 1968.
- (35) Somorjai, G. A. *Introduction to Surface Chemistry and Catalysis*; John Wiley and Sons: New York, 1994.

EXPERIMENTAL

2.1 Survey of Analytical Techniques

X-ray photoelectron spectroscopy (XPS) is frequently used to determine the chemical composition of a surface.^{1,2} The technique is based on the photoelectric effect. When a surface is exposed to photons of sufficient energy, electrons will be ejected from that surface with a specific kinetic energy. These are commonly called photoelectrons. The kinetic energy a photoelectron possesses depends on the energy of the incident photon, the core-level energy-state from which the electron was removed and the workfunction of the material. The photoelectrons are then energy analyzed and their binding energies determined using the following expression.

$$KE = hv - E_b - \phi \tag{1}$$

Here hv is the energy of the incident photon (usually K α lines of Al or Mg at hv = 1486.6 and 1253.6 eV, respectively), E_b is the binding energy of the electron in the sample and ϕ the workfunction of the material.³ This process is outlined in Figure 2.1. Note that for a solid surface, the photon energy must exceed the sum of the binding energy of the electron at its core-energy level and the workfunction of the surface. The chemical composition of a surface is determined from the fact that each element displays a unique set of binding energies.

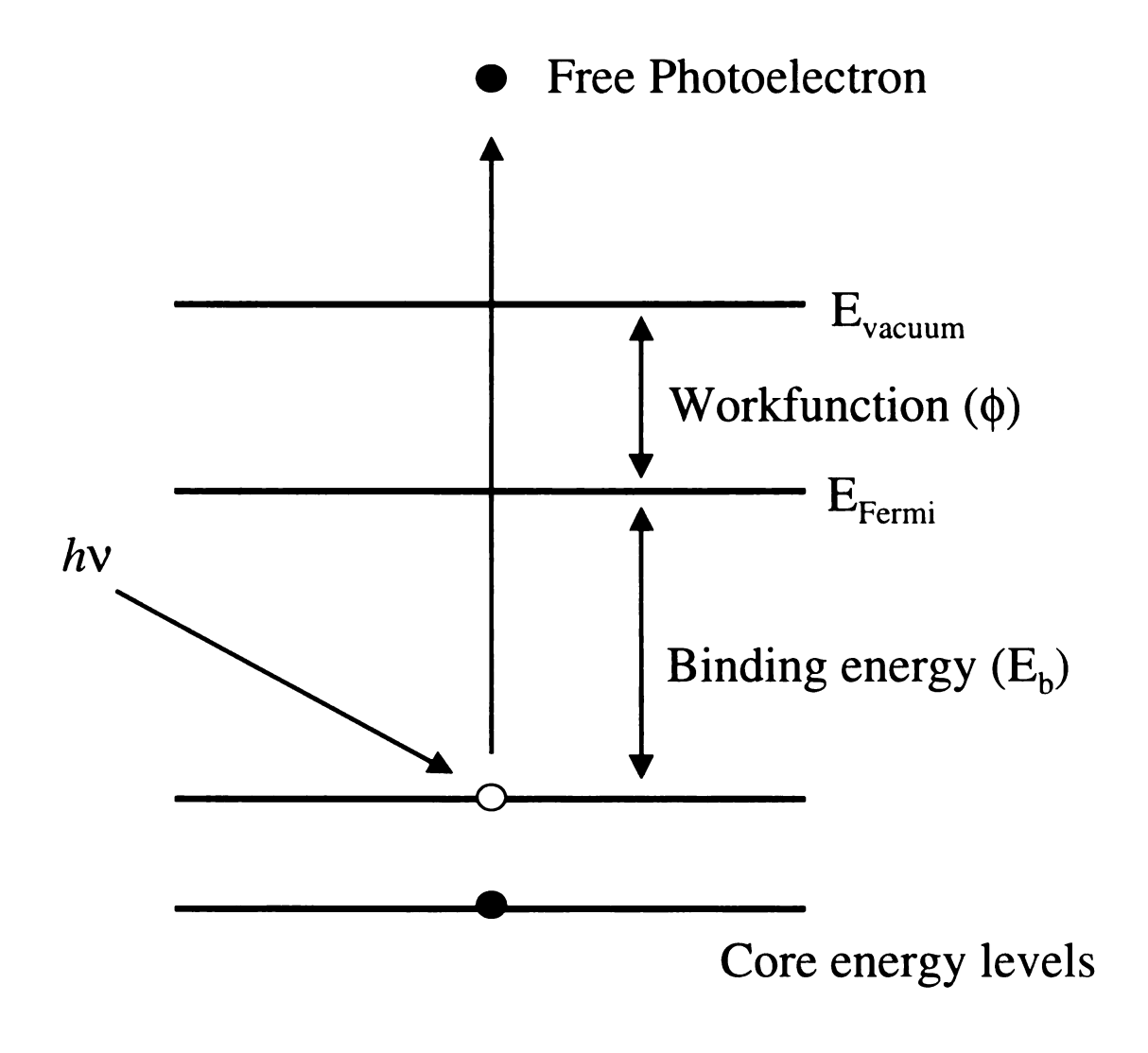


Figure 2.1 Schematic diagram of X-ray photoelectron generation.

X-ray photoelectron spectroscopy has high surface sensitivity, probing no more then 100 Å into the surface.⁴ This is due to the short inelastic mean free path a photoelectron will travel in a solid material. Only photoelectrons that have been generated within the local surface region can escape the surface to be energy analyzed. Therefore, XPS gives an accurate description of the near-surface composition.

Temperature programmed desorption (TPD) is commonly employed to gain information about the energetics and coverage of molecules adsorbed on a solid surface. 5 It can be envisaged that a molecule adsorbed at a surface lies in a potential well of depth E_d (E_d = desorption energy). The temperature of the sample is then raised linearly as a function of time and at some temperature the adsorbed molecules will obtain enough energy to break the adsorbate-surface bond and desorb from the surface. A quadrupole mass spectrometer is used to measure the rate that the molecules desorb from the surface. The rate is expressed as an Arrhenius type expression called the Polanyi-Wigner equation (2).

$$- dn / dt = n^{x} v_{x} \exp(-E_{d}/RT)$$
 (2)

In this expression x represents the "order" of desorption, n is the number of molecules, v is a frequency factor and E_d is the desorption energy. This expression can then be fit to the experimental data to give information about the magnitude of the adsorbate-surface bond (E_d). If E_d is less than 40 kJ/mol the adsorbate is considered to be physisorbed on the surface; in other words no true chemical bond has formed between the adsorbate the surface. Desorption energies greater than 40 kJ/mol suggest the adsorbate forms a true chemical bond with the surface, and this process is termed chemisorption.⁶

The peak shape of TPD spectra can be used to describe both coverage and desorption mechanisms. Because the chemical environment of monolayer and multilayer adsorbates is usually different, often two separate desorption peaks will appear in a TPD spectrum at coverages greater than 1 monolayer. The first monolayer typically desorbs with first order kinetics, implying that the desorption rate depends linearly on coverage. In this case the temperature at the maximum rate of desorption remains constant with respect to coverage, and the peak is typically asymmetric in shape. If interaction between the first monolayer and subsequent monolayers is weaker than the first monolayer-substrate interaction then multilayer adsorbates will desorb at a lower temperature than the monolayer. It is common for multilayer desorption to follow zero order desorption kinetics. Here, the desorption rate doesn't depend on coverage but increases exponentially with temperature. Second and fraction order desorption mechanisms are known but are rare and will not enter into this study of butadiene on HOPG(0001).

High-resolution electron energy loss spectroscopy (HREELS) is used to probe molecular vibrations of adsorbates on a surface. ^{1,8} High sensitivity (able to detect 1% of a monolayer) and broad applicability have made HREELS an invaluable surface sensitive analytical technique. The technique works by scattering a monoenergetic beam of electrons (1-15 eV) from a surface at a specific angle. The scattered electrons are then energy analyzed. Most of the electrons will scatter elastically, but some will lose energy and scatter inelastically. These inelastically scattered electrons undergo energy losses corresponding to the energy of molecular vibrations on the surface. ⁹ There are three scattering mechanisms: dipole scattering, impact scattering, and negative ion resonance

scattering. Dipole scattering is the most common and is the mechanism from which the data will be obtained in this study.

Dipole scattering results when an electron approaching the surface is influenced by an oscillating dipole. Only dipoles perpendicular to the surface affect the electron, since a dipole that is perpendicular to the surface is enhanced by its image dipole within the surface. A dipole parallel to the surface is cancelled by its image in the surface. This provides the "surface selection rule" that states that only vibrations perpendicular to the surface will been seen in an HREELS spectrum (see Figure 2.2). Vibrations parallel to the surface will not be seen by dipole scattering. Using this information, one can qualitatively determine the orientation of an adsorbate on a surface.

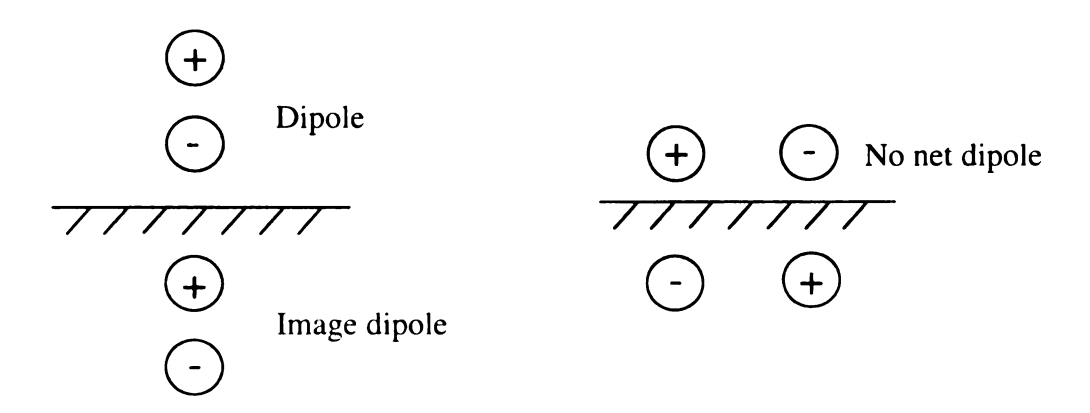


Figure 2.2 Representation of a dipole perpendicular to a surface and its image dipole in the surface (left) and a dipole parallel to a surface plane with its mirror image in the surface (right).

2.2 Experimental Apparatus

All experiments were carried out in two connected stainless steel ultrahigh vacuum (UHV) chambers, each one containing a 270 L/s ion pump to maintain ultrahigh vacuum. The first chamber also contained a molecular leak valve, a 0-200 amu quadrupole mass spectrometer, and an X-ray source and hemispherical electron energy analyzer for X-ray photoelectron spectroscopy (XPS). The second chamber contained a high-resolution electron energy loss spectrometer. The base pressure of the chamber was 1.6x10⁻¹⁰ torr.

Highly ordered pyrolytic graphite (HOPG) (grade SPI-2, SPI supplies) with approximate dimensions of 10x10x1 mm was fastened to a molybdenum sample mount using molybdenum clips. Before introduction to the UHV chamber, the HOPG sample was peeled using adhesive tape. An E-type thermocouple was placed between the HOPG sample front face and a molybdenum clip. The sample could be cooled to 77 K using liquid nitrogen or heated to ~800 K via a tungsten filament embedded in the mount. The sample holder was also capable of x, y, and z translation and θ rotation. Following bakeout, the sample was annealed to 700 K for several hours in order to remove any contaminates present on the surface.

After annealing the sample, the surface composition was monitored using XPS. All XPS data were collected using the Al K α X-ray line (hv=1486.6 eV) operated at 300 W (15 kV and 20 mA). The pass energy of the spectrometer was set at 100 eV, and XPS data were measured collected at a take-off angle of 45° from the surface normal in order to increase surface sensitivity. The surface of the HOPG sample was found to be free of all species other than carbon except for ~1.0% of an oxygen species that could not be removed. A survey scan of the annealed sample surface is shown in Figure 2.3. The

large peak in the spectrum at 286 eV is due to photoelectron emission from the carbon 1s orbital. The only other identifiable feature in the spectrum is due to the emission from the oxygen 1s orbital centered at 533 eV.

An excimer laser (Questek 2440) operating at 193 nm (ArF), 248 nm (KrF) or 351 nm (XeF) was used to provide UV photons. The laser was operated at an average power of 0.5 W at all wavelengths and a repetition rate of 5 Hz. The laser pulse duration (FWHM), quoted by the laser manufacturer, was 8-16 ns. The laser light was passed through a quartz window on the UHV chamber and impinged on the sample at 45° from surface normal, (see Figure 2.4). All irradiation experiments were performed at < 85 K.

1,3-Butadiene gas (Aldrich 99%) was used without further preparation. The gas was introduced to the UHV chamber via a stainless steel manifold coupled to a molecular leak valve. The gas was dosed onto the sample through a 1/8" inside diameter stainless steel tube (the "directed doser"). In order to expose the sample to butadiene consistently, the leak valve was opened and mass 39 (C₃H₃⁺), the most abundant ion in the gas phase cracking pattern of butadiene, was measured with the mass spectrometer. Once a predetermined constant signal was obtained, the sample was placed in front of the directed doser (~5 mm from the sample surface) for a specified amount of time.

Temperature-programmed desorption (TPD) experiments were performed by positioning the surface in light-of-sight of the 2 mm entrance aperture of a shrouded mass spectrometer. The electron impact ionization source was operated at 70 eV and a bias of > -70 V was placed on the sample in order to repel any electrons from the ion source of the mass spectrometer. During TPD experiments, the sample was linearly heated at a rate

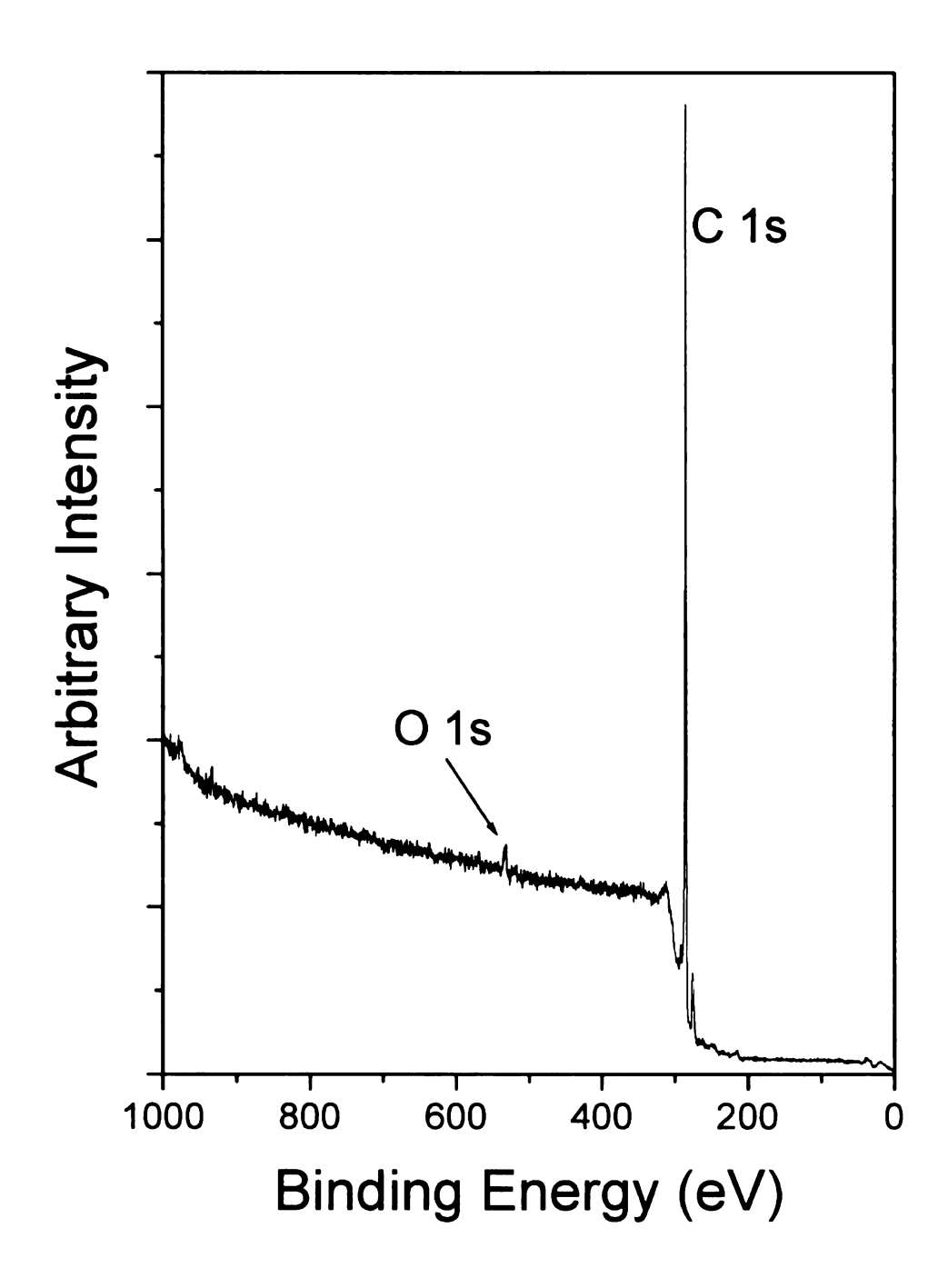


Figure 2.3 X-ray photoelectron spectrum of the HOPG surface before experiments.

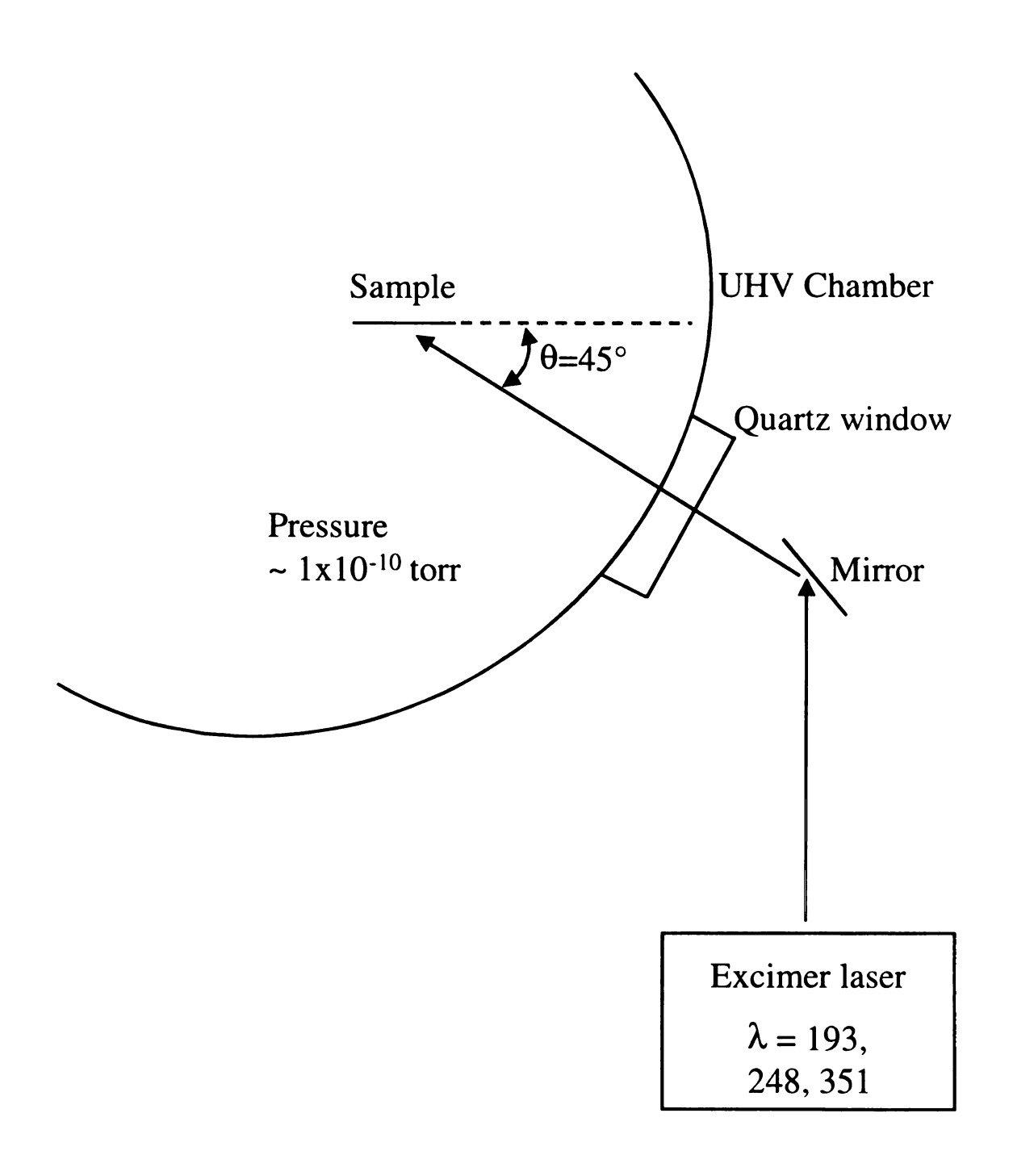


Figure 2.4 Experimental apparatus showing Excimer laser and UHV chamber orientation.

of 5 K/s up to a maximum temperature of 450 K. A fresh layer of butadiene was prepared for each experiment.

The adsorption and photochemistry of butadiene was also characterized using EELS. The scattering angle in our spectrometer was set to $\theta_i = 55^\circ$, and all data presented in this study was collected 1° off-specular ($\theta_s = 56^\circ$) to slightly reduce the intense inelastic scattering background from the semi-metallic graphite surface. The intensity of this inelastic background decreases quickly as the scattering geometry moves away from the specular direction. The primary beam energy was 6.1 eV and resolution from the $C_4H_6/HOPG$ surface was between 36 and 44 cm⁻¹ as determined from the elastic peak FWHM for all data shown here.

2.3 References

- (1) Perry, S. S.; Somorjai, G. A. Analytical Chemistry **1994**, 66, 403 A.
- (2) Woodruff, D. P.; Delchar, T. A. *Modern Techniques of Surface Science*, 2nd ed.; Cambridge University Press: Cambridge, 1994.
- (3) Handbook of X-ray Photoelectron Spectroscopy; Wagner, C. D.; Riggs, W. M.; Davis, L. E.; Moulder, J. F., Eds.; Perkin-Elmer Corporation: Eden Prairie, 1979.
- (4) Briggs, D.; Seah, M. P. *Practical Surface Analysis*, 2nd ed.; Wiley: New York, 1990; Vol. 1-Auger and X-ray Photoelectron Spectroscopy.
- (5) King, D. A. Surf. Sci. 1975, 47, 384.
- (6) Somorjai, G. A. *Introduction to Surface Chemistry and Catalysis*; John Wiley and Sons: New York, 1994.
- (7) Jong, A. M.; Niemantsverdriet, J. M. Surf. Sci. 1990, 223, 355.
- (8) Sexton, B. A. Appl. Phys. A **1981**, 26, 1.
- (9) Ibach, H.; Mills, D. L. Electron Energy Loss Spectroscopy and Surface Vibrations; Academic Press: London, 1982.
- (10) Palmer, R. E.; Annett, J. F.; Willis, R. F. Surf. Sci. 1987, 189/190, 1009.

ADSORPTION AND PHOTOCHEMISTRY OF 1,3-BUTADIENE ON HOPG

3.1 Adsorption of Butadiene on HOPG determined by TPD

The adsorption of butadiene on HOPG(0001) was studied using temperature programmed desorption. Figure 3.1 shows TPD (m = 39, C₃H₃⁺) profiles for various exposures of butadiene adsorbed on HOPG at < 85 K. The first monolayer of butadiene on HOPG displays apparent first-order desorption kinetics and desorbs with a maximum rate at about 129 K. Using Redhead analysis,¹ the desorption energy was determined to be 32 kJ/mol, suggesting that butadiene is physisorbed on the HOPG surface. With increased butadiene exposure, a second feature appears, initially located with a maximum rate of desorption at 105 K. This feature is ascribed to second and multilayer desorption since it does not saturate at large exposures. Multilayer desorption shows zero-order desorption kinetics with an activation energy determined by leading edge analysis² to be 28.5 kJ/mol.

Interestingly, the monolayer peak does not saturate as the multilayer peak begins to grow in. When the monolayer peak becomes saturated, approximately 16% of the total number of adsorbed molecules are associated with the multilayer peak. This indicates that butadiene is probably forming 3-D islands on the HOPG (0001) surface before the first monolayer is complete. In this work one monolayer (ML) is defined as the maximum coverage of butadiene on HOPG where no multilayer desorption is seen by TPD. This coverage represents approximately 83% of the saturated monolayer coverage.

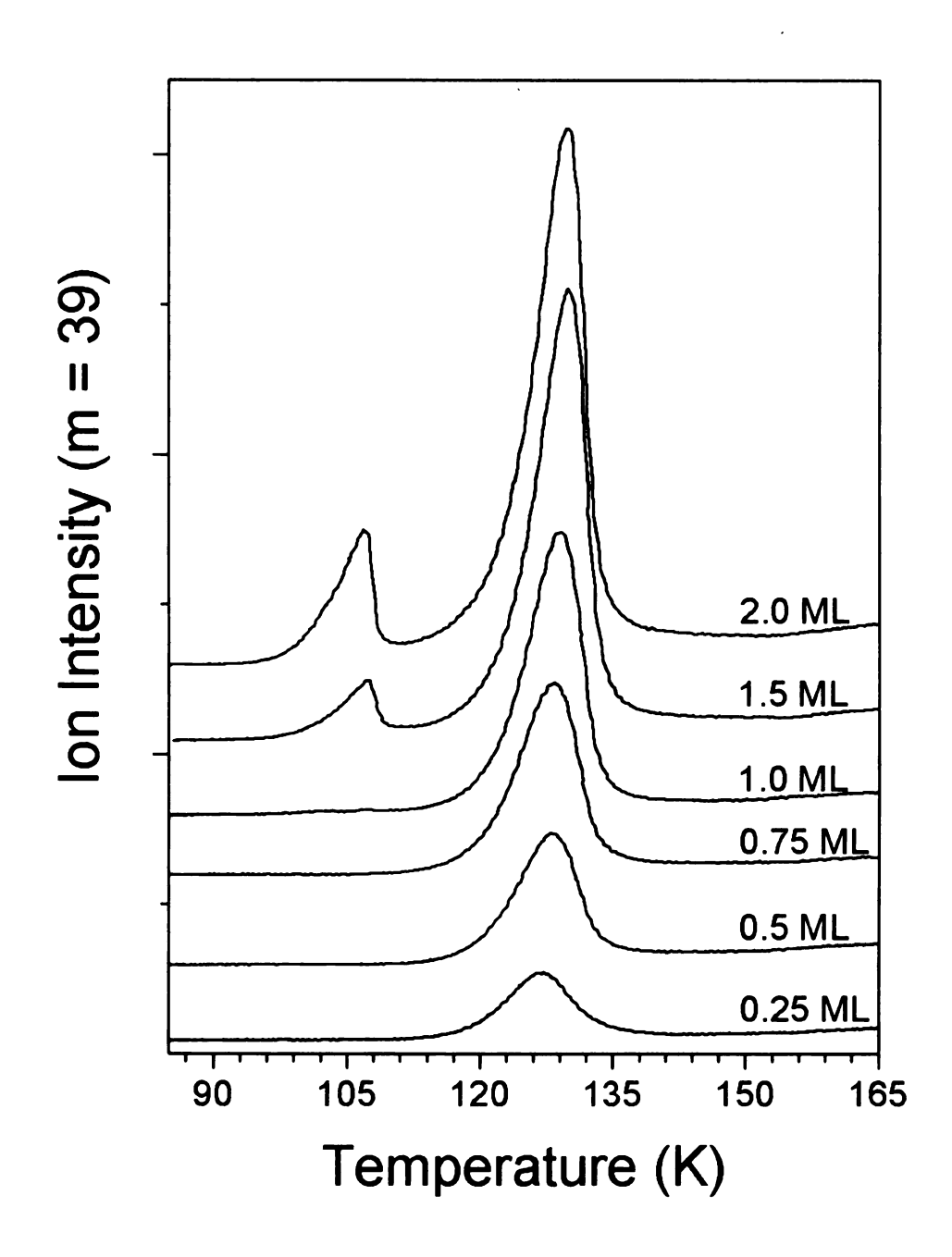


Figure 3.1 Mass $(C_3H_3^+)$ thermal desorption spectra of C_4H_6 on HOPG with increasing coverage. At 2.0 ML coverage the 1st monolayer is saturated.

To confirm butadiene desorbs molecularly, further TPD experiments were performed. Figure 3.2 shows TPD spectra for several butadiene fragment masses (m = 39 $C_3H_3^+$, m = 27 $C_2H_3^+$, and m = 54 $C_4H_6^+$) at a constant coverage of 1.0 ML. The area under each desorption peak was calculated and compared to the relative intensity for each mass in the gas phase cracking pattern of butadiene (see appendix). In the gas phase mass spectrum of butadiene, mass 39 is the most abundant ion and the relative intensities of mass 27 and 54 are 80% and 55% respectively. The TPD data corresponds closely with the gas phase cracking pattern with mass 27 and 54 at 75% and 51%, respectively, of the mass 39 area. The similarity of the gas phase and desorbed molecule fragmentation patterns indicates that no measurable irreversible adsorption occurred.

3.2 Adsorption of Butadiene on HOPG determined by EELS

Electron energy loss spectroscopy (EELS) was also used to study the adsorption of butadiene on HOPG. Figure 3.3a shows an EELS spectrum for 1 ML of butadiene adsorbed on HOPG at < 85 K. The spectrum shows several distinct loss features and assignment of these peaks by comparison with IR literature data ³ suggests that the planar butadiene molecule adsorbs, with its mirror plane containing all atoms, parallel to the HOPG surface plane without significant C atom rehybrization. Based upon both the IR frequency assignments between the *cis* and *trans* isomers, ⁴ and knowing that at room temperature less than 1% of gaseous butadiene molecules are in the *cis* conformation, ⁵ the adsorption isomer of butadiene on HOPG is proposed to be the *trans* conformation. Frequency shifts in IR spectra associated with the *trans* and *cis* isomers will be discussed

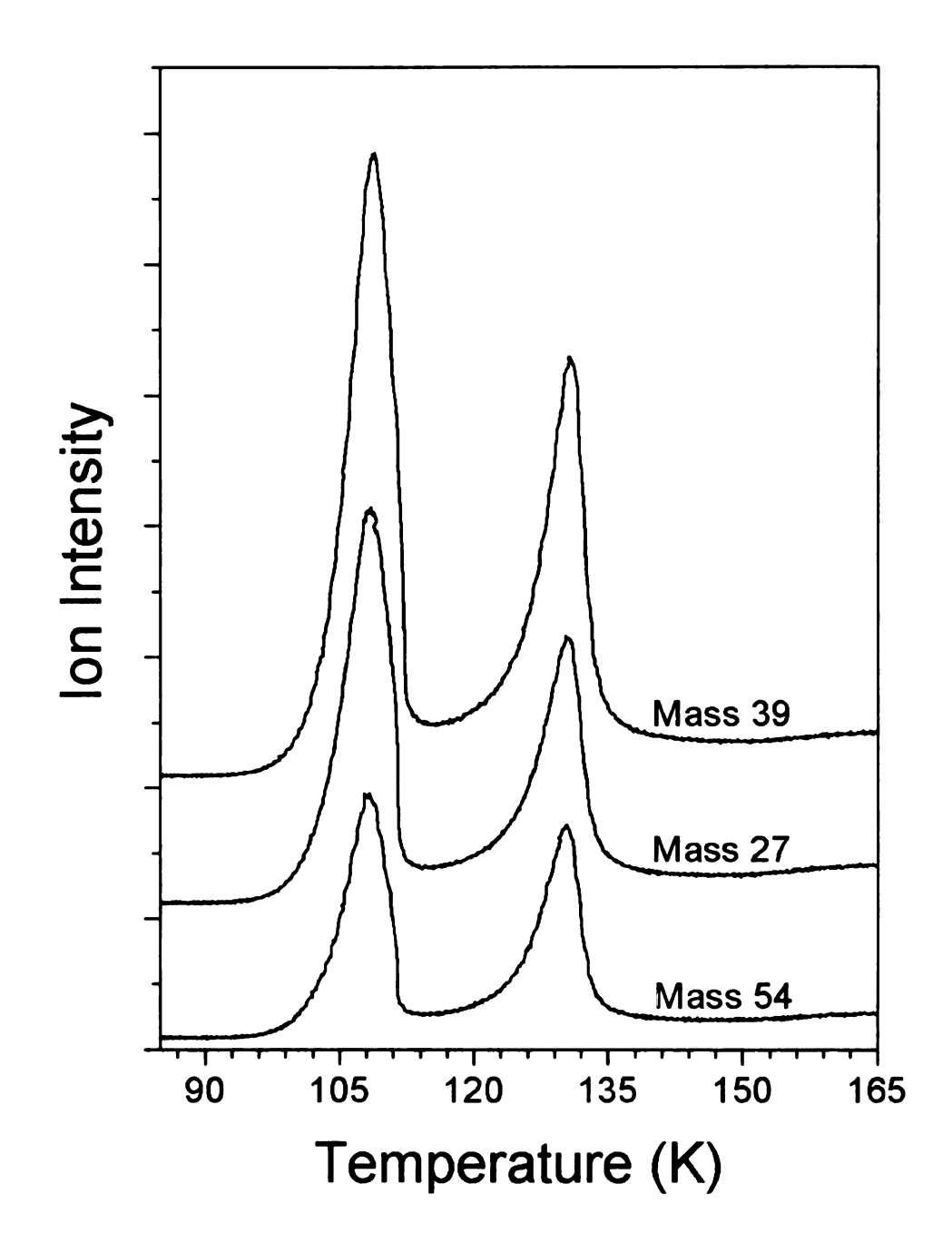


Figure 3.2 Thermal desorption spectra for masses 39 $(C_3H_3^+)$, 27 $(C_2H_3^+)$ and 54 $(C_4H_6^+)$ of C_4H_6 on HOPG for \leq 3 ML coverage to ensure the 1st monolayer is saturated.

further below. The features visible in the EEL spectra of 1,3-butadiene(ad)/HOPG are the ρ_t (torsion between C_2 and C_3) at ~186 cm⁻¹, the ρ_t (=CH₂ twist) at 532 cm⁻¹, the ω (CH₂ wag) at 909cm⁻¹, the ω (CH bend) at 1014 cm⁻¹, and the v (CH stretch) at 3025 cm⁻¹ ¹. All of the observed losses in the EEL spectrum belong to out-of-plane vibrations except for the v (CH) mode at ~3025 cm⁻¹. The appearance of the v (CH) mode is believed to be due to the low frequency torsion mode at ~186 cm⁻¹ that lowers the symmetry of the molecule away from C_{2h} , moves the C-H motion away from parallel to the surface plane and allows it to be seen by EELS. The butadiene adsorption geometry is also supported by the absence of several in-plane IR active molecular vibrations (for example, the v (C=C stretch) at 1596 cm⁻¹ and the δ (=CH₂ in plane bend) at 1381 cm⁻¹) that would be screened in the parallel geometry. The ρ_t (=CH₂ twist) at 532 cm⁻¹ indicates that butadiene adsorbs onto HOPG in the trans conformation. In the cis conformation the p₁ (=CH₂ twist) shifts to about 730 cm⁻¹.⁴ Similar conclusions about the adsorption geometry and conformation were reached in studies of butadiene on Au(111).6 There is no evidence for the formation of cycle-type adsorbates on graphite as have been proposed on some metal surfaces where interaction between the butadiene and the surface leads to significant double bond activation.⁷

Electron energy loss spectroscopy was also used to investigate multilayer (3 ML) adsorption of butadiene on HOPG (see Figure 3.3b). The multilayer data is very similar to the monolayer data; all of the same peaks appear at approximately the same frequency, but with an increased signal to noise ratio. No new peaks appear in the multilayer spectrum and the ratio of intensities between the various features is very similar to that of the monolayer. I believe that these data indicate that butadiene forms

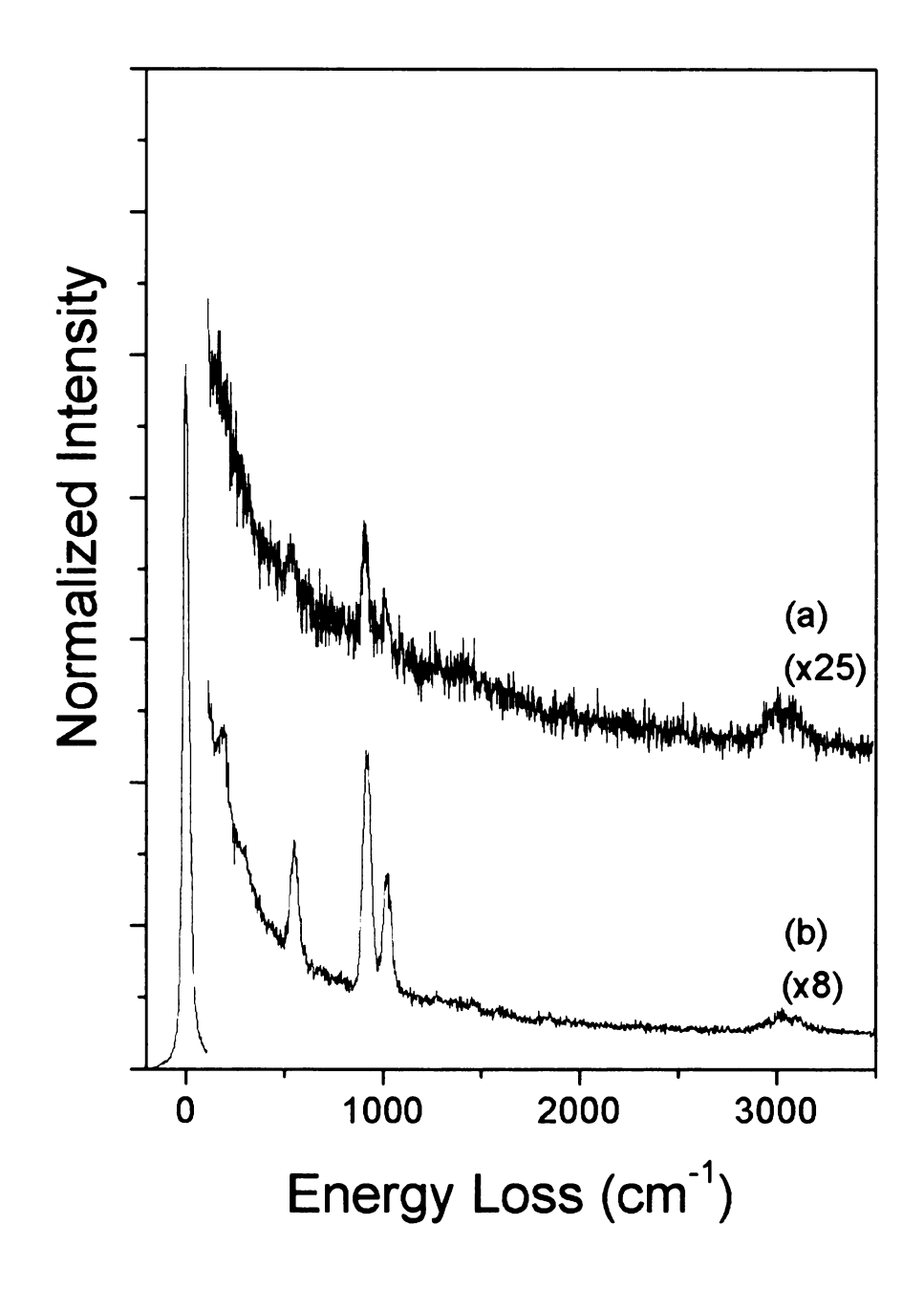


Figure 3.3 Electron energy loss spectroscopy of (a) 1 ML and (b) 3 ML C_4H_6 on HOPG.

Normal vibrational modes	Gas phase frequencies (cm ⁻¹)	EELS 1 ML C ₄ H ₆ /HOPG (cm ⁻¹)	EELS 3 ML C ₄ H ₆ /HOPG (cm ⁻¹)
C-C torsion (a _u)	162.3	186	186
CCC deform (a _g , b _u)	512 ^a , 301		
CH_2 twist (a_u, b_g)	522, 770 ^a	532	550
CH_2 wag (a_u, b_g)	908, 912 ^a	909	919,
CH bend (a_u, b_g)	1013, 976°	1014	1021
C-C str (a _g)	1196 ^a		
CH bend (a _g , b _u)	1280°, 1294		
CH ₂ scis (a _g , b _u)	1438 ^a , 1294		
$C=C str(a_g, b_u)$	1630°, 1596		
CH_2 s-str (a_g, b_u)	2992 ^a , 2984	3025 ^b	3043 ^b
CH str (a_g, b_u)	3003 ^a , 3055	3025 ^b	3043 ^b
CH ₂ a-str (a _g , b _u)	3087 ^a , 3101	3025 ^b	3043 ^b

Table 3.1 Vibrational assignments of 1,3-butadiene adsorbed on HOPG(0001).

^a IR inactive mode
^b Not able to deconvolute based on the resolution of EELS

ordered multilayers on top of the first monolayer, with a similar parallel adsorption geometry to that of the monolayer. The peak maxima for all EELS data are listed in Table 3.1 along with IR values for $C_4H_6(g)$.

3.3 Photodesorption of Butadiene monitored by TPD

Figures 3.4 and 3.5 show TPD results (mass 39) for 1 ML (Figure 3.4) and 3 ML (Figure 3.5) of butadiene adsorbed onto HOPG at < 85 K following irradiation with 193 nm photons at incident energies of 100 mJ/pulse. Irradiating the adlayer with 3x10¹⁷ photons/cm² resulted in a decrease in molecularly adsorbed butadiene as indicated by the loss of intensity for mass 39 in the TPD data shown. Continued irradiation further decreases the butadiene coverage as clearly seen in Figure 3.4, where after irradiating the butadiene monolayer with 5x10¹⁹ photons/cm², only 18 % of the initial monolayer remained on the surface. The temperature of the maximum rate of desorption and peak shape remained constant for all TPD data collected. Furthermore, mass spectra from 0-100 amu collected during TPD showed no desorbing fragments other than those belonging to butadiene.

Figure 3.5 shows the same data as for Figure 3.4, but with 3 ML coverage of butadiene on HOPG. Irradiation of the adsorbate layers produces a decrease in the mass 39 signal for both monolayer and multilayer peaks. Measurements at other masses confirmed that, as for the monolayer, the only significant specie remaining on the surface following irradiation of the multilayer was butadiene. There was no evidence for reaction products remaining adsorbed, implying that butadiene desorbs molecularly (without

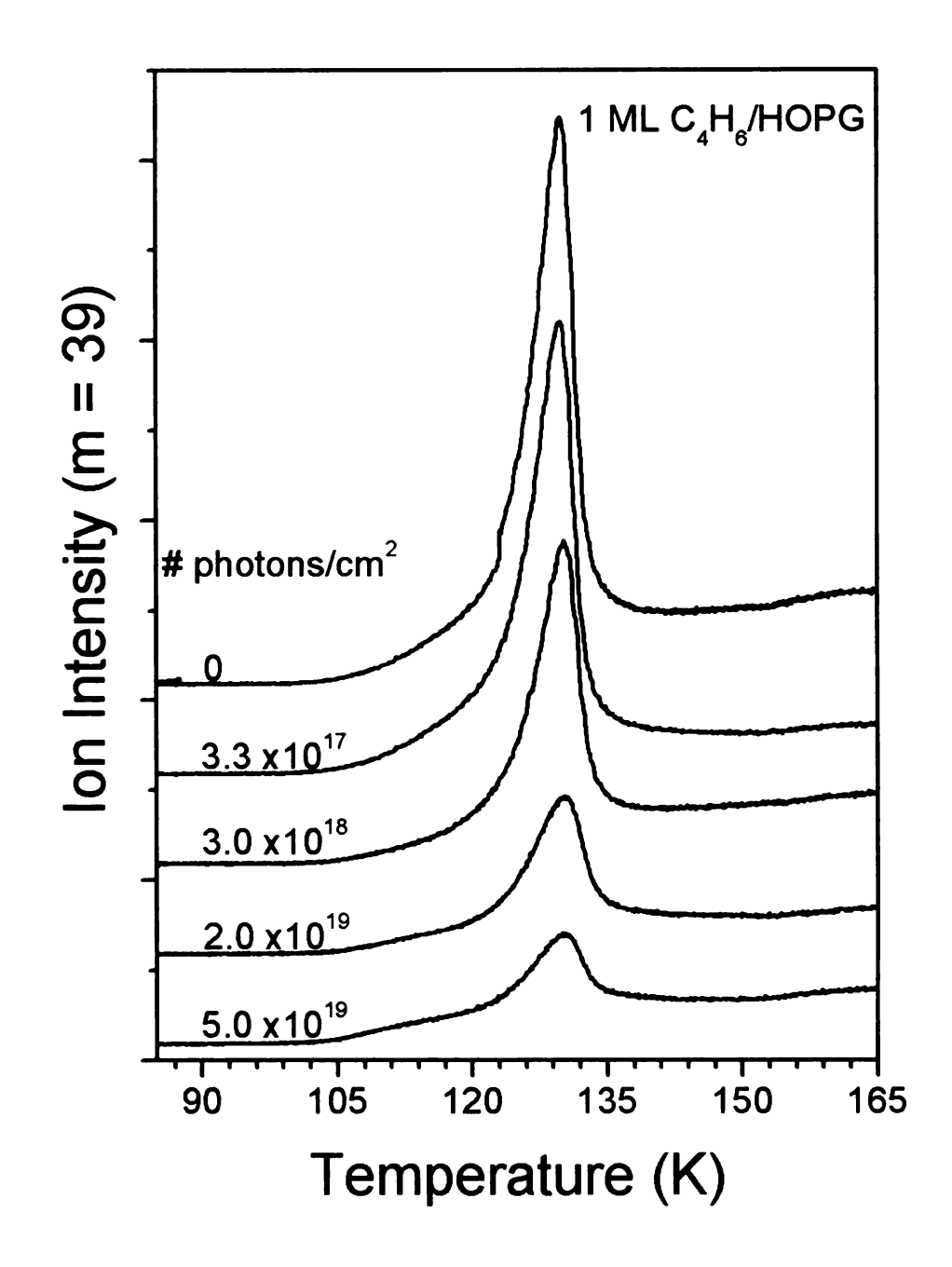


Figure 3.4 Thermal desorption spectra (mass 39, $C_3H_3^+$) of 1 ML C_4H_6 on HOPG irradiated with increasing photon number ($\lambda = 193$ nm).

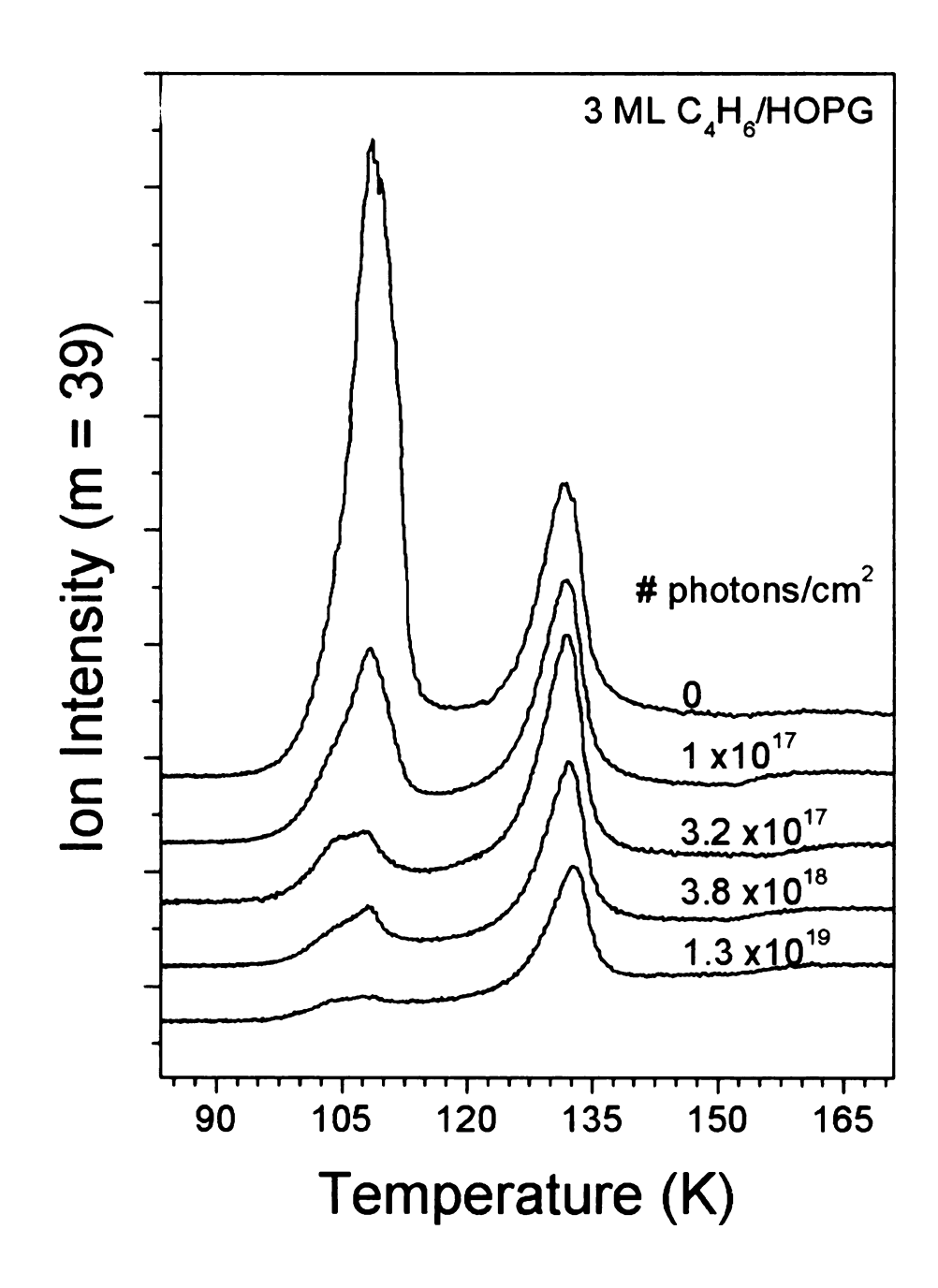


Figure 3.5 Thermal desorption spectra (mass 39 $C_3H_3^+$) of 3 ML C_4H_6 on HOPG irradiated with increasing photon number ($\lambda = 193$ nm).

fragmentation) from the surface. The multilayer peak intensity decreases at a faster rate than the monolayer peak intensity, as will be discussed further below.

In order to quantify the photodesorption process, the area under each desorption peak was calculated. Assuming that the process follows first order kinetics, a plot of $\ln(C_4H_6)$ (I)/ C_4H_6 (II) vs. total incident photon number (n_{ph} photons/cm²), where C_4H_6 (II) is the area under a TPD peak after a specific total incident photon number and C_4H_6 (II) is the area under the TPD peak for an unirradiated adlayer, should give a straight line. The slope of the line is equal to the cross section σ (cm²/photon) for photodesorption. Figure 3.6 shows a semi-logarithmic plot of TPD area vs. total incident photon number for the data shown in Figure 3.4. The total cross section for photodesorption was calculated to be 3.3×10^{-20} cm² at 193 nm and 100 mJ/pulse. The cross section for 3 ML coverage was calculated to be 1×10^{-17} cm², about three orders of magnitude greater than the 1 ML cross section. The experiment was repeated at 248 nm and 351 nm for both 1 ML and 3 ML coverages. Table 3.2 lists all of the cross sections calculated here along with the gas phase cross sections of absorption at the various wavelengths.

Wavelength (nm)	1 ML cross section	3 ML cross section	Gas phase
	(cm ²)	(cm ²)	cross section (cm ²) ¹¹
193	$3.3x10^{-20}$	1.1x10 ⁻¹⁷	4x10 ⁻¹⁷
248	2.4×10^{-20}	6.3×10^{-18}	$2x10^{-19}$
351	1.2×10^{-20}	1.8×10^{-18}	~0

Table 3.2. Butadiene photodesorption cross sections and gas phase cross sections from the literature.

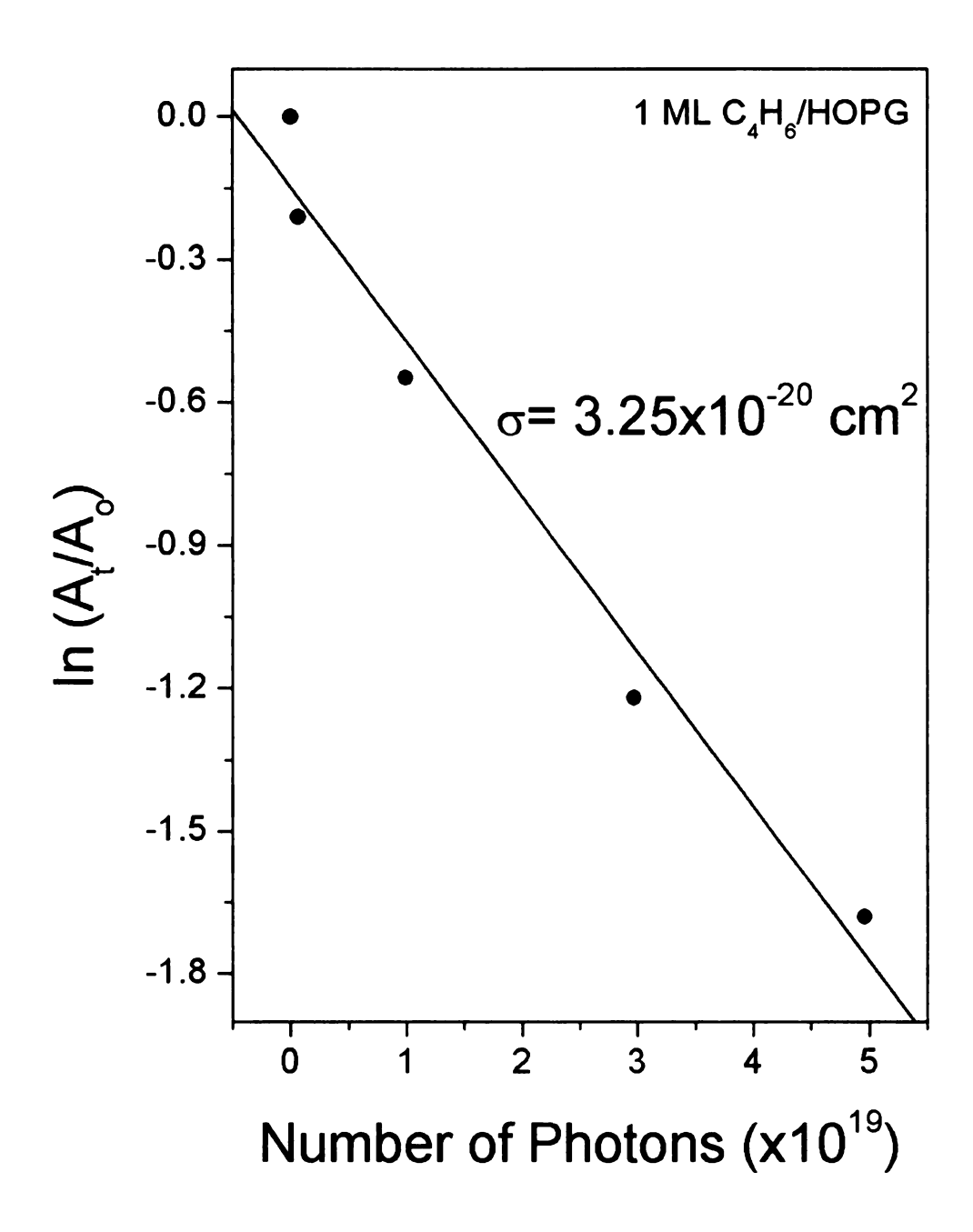


Figure 3.6 Semi-logarithmic plot of TPD peak area vs. total number of photons/cm² for calculation of the photodesorption cross section.

3.4 Photodesorption of Butadiene monitored by EELS

Electron energy loss spectroscopy was also used to examine the 193 nm photochemistry of 1 ML butadiene on HOPG. For all total incident photon numbers up to $5x10^{19}$ photons/cm², identical features to those observed for the unirradiated monolayer were observed. The general loss in peak intensities and the decrease in signal-to-noise ratio with prolonged irradiation, coupled with the pronounced inelastic background of graphite made it difficult to determine the energy loss peak positions with confidence. No new peaks appeared in the EELS data with prolonged irradiation, suggesting that no adsorbed state reaction products were created in measurable quantities, in accord with the TPD data discussed above.

The increased signal-to-noise ratio of the EELS data for multilayer butadiene exposures allowed us to more reliably investigate changes in the EEL spectra with irradiation. Figure 3.7 shows the vibrational spectrum obtained by irradiating 3 ML of butadiene adsorbed on HOPG with 1x10¹⁷ photons/cm² at 193 nm and 100 mJ/pulse. Clearly, the presence of loss features indicates that a substantial amount of butadiene remained adsorbed on the surface (TPD data suggested that approximately 2 ML are present on the surface following this photon exposure). Once again, no new features were observed in the EELS data due to the accumulation of adsorbed products.

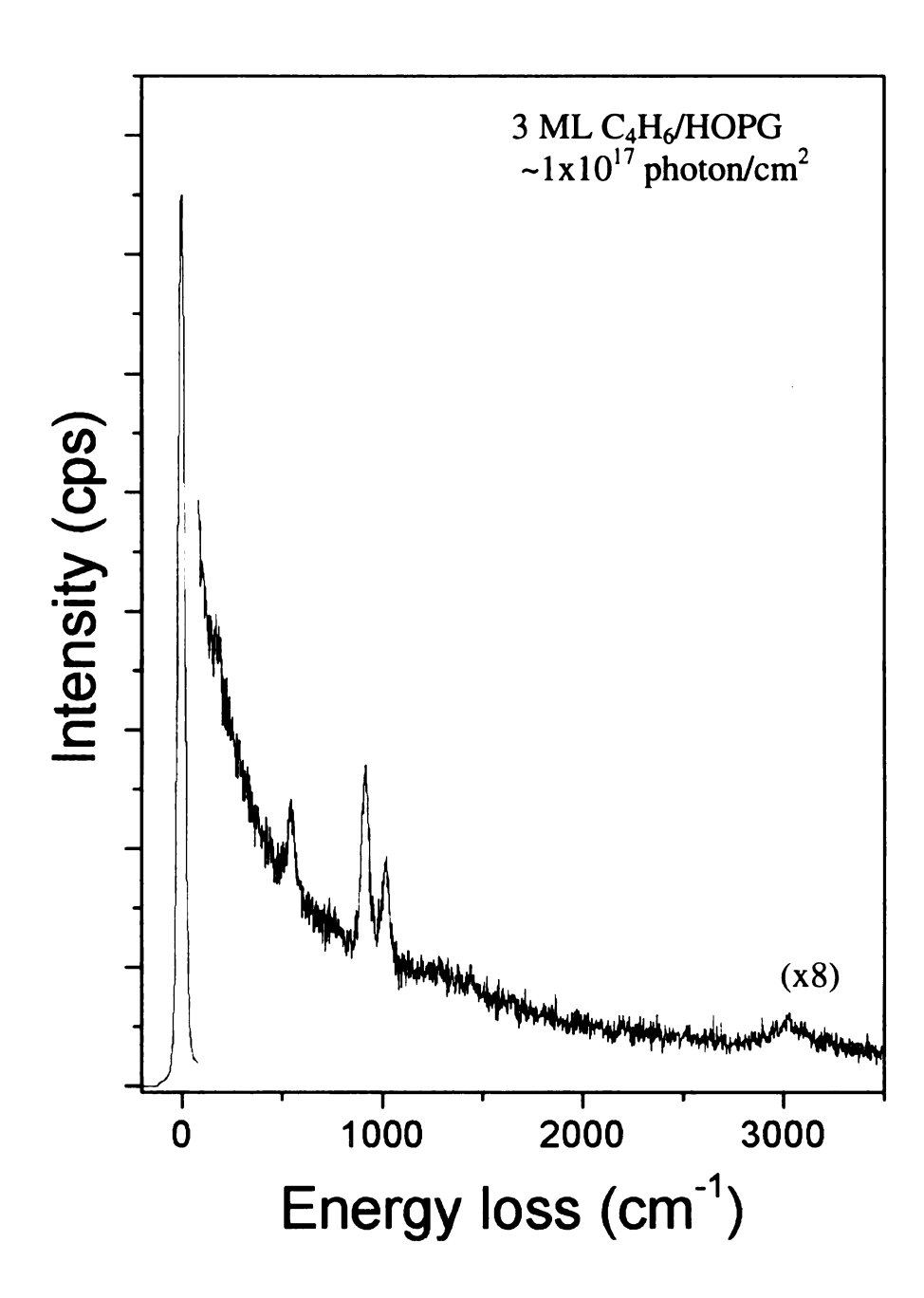


Figure 3.7 Electron energy loss spectra of 3 ML C_4H_6 on HOPG exposed to $1x10^{17}$ photons/cm².

DISCUSSION

3.5 Mechanisms for Photodesorption

Over the past 15 years, several photodesorption mechanisms have been proposed in the literature. Each will be briefly discussed in relation to the experimental data presented here. The three mechanisms considered are: (1) an adsorbate-mediated process, commonly called photodesorption or photoejection, involving the direct absorption of a photon by an adsorbate molecule or adsorbate-substrate complex; (2) a substrate-mediated process involving the absorption of a photon by the surface and electronic energy transfer to the adsorbate-substrate bond; and (3) laser-induced thermal desorption (LITD) which occurs when energy absorbed by the surface is quickly converted to surface phonons, and the local surface temperature rise causes desorption. For a more in-depth discussion of these processes, the reader is referred elsewhere.⁸⁻¹⁰

3.6 Adsorbate-mediated Processes

Gas-phase butadiene absorbs UV radiation from about 170 nm to 225 nm. 11 The wavelength of maximum absorption is 210 nm where the cross section is 1×10^{-16} cm 2 . 12 In this wavelength range, absorption results in a $\pi \rightarrow \pi^*$ transition to two closely spaced states (the $1B_u$ and $2A_g$ states). These states have lifetimes of < 100 fs, and decay from these states eventually leads to single-bond isomerization in about 270 fs. 13

In general, adsorbate molecule-mediated surface photochemical processes exhibit a wavelength dependence that is qualitatively similar to absorption by the analogous gas phase molecule. As such, if the photodesorption of butadiene on graphite is initiated by direct adsorbate absorption, we might expect it to be a maximum near 193 nm, to

decrease significantly at 248 and be negligible at 351 nm. The gas phase absorption cross sections for butadiene are $\sim 4 \times 10^{-17}$ cm², $< 2 \times 10^{-19}$ cm² and essentially zero at 193 nm, 248 nm and 351 nm, respectively. If we compare these values with the cross sections for photodesorption for 1 ML of butadiene on HOPG, 3.3×10^{-20} cm², 2.4×10^{-20} cm² and 1.2×10^{-20} cm² at 193 nm, 248 nm and 351 nm, respectively, we find a poor correlation between the photodesorption and gas-phase cross sections. It is not uncommon for the photochemical response of adsorbed molecules to be red shifted by up to 1 eV from the gas-phase spectrum, but the absorption spectrum remains qualitatively similar.

Although the cross sections for photodesorption from 3 ML of $C_4H_6(ad)/HOPG$ are about two orders of magnitude higher than those for 1 ML of $C_4H_6(ad)/HOPG$, the variation with wavelength is very similar to the 1 ML case. For both mono and multilayer coverages, it appears that photodesorption is not dominated by adsorbate absorption.

3.7 Substrate-mediated Processes

Photochemical processes driven by initial photon absorption by the surface have been commonly reported for metal and semiconductor substrates. They originate when electrons generated in the near-surface region migrate and attach to molecular orbitals within the adsorbed molecule or adsorbate-substrates complex. Two cases are often described. In the first, the incident photon energy exceeds the workfunction of the material and true photoelectrons are produced. In the second process, the incident photon energy is less than the workfunction of the material and so-called 'hot' or sub-vacuum

level electrons are generated. These can tunnel into the adsorbate depending upon the energetic and spatial arrangement of the surface and adsorbate energy levels.

We discount the production of free photoelectrons as being responsible for the desorption of butadiene based upon the workfunction of graphite of 4.4 eV.¹⁴ Assuming that the workfunction does not change considerably upon adsorption (sensible for a physisorbed system), photoelectrons cannot be generated for incident wavelengths greater than about 280 nm. However, we observe appreciable photodesorption at 351 nm in our experiments, and so discount photoelectron effects as dominating the photodesorption of butadiene from HOPG.

Subvacuum-level or 'hot' electrons are undoubtedly created at all wavelengths used in our work. However, we do not believe that they are responsible for the observed photodesorption of butadiene. Other studies have indicated that the mean free path of these hot electrons is limited to only a few layers of an adsorbate. Regardless, in the absence of additional quenching routes operative in the first adsorbed layer, a hot electron driven desorption process should produce a much greater rate of desorption for the adsorbate layer in contact with the surface than for subsequent multilayers. Since we observe a multilayer photodesorption rate that is some two orders of magnitude greater than the monolayer photodesorption rate at all wavelengths, we conclude that hot electrons are not contributing significantly to butadiene desorption.

3.8 Laser-induced Thermal Desorption

Laser-induced thermal desorption (LITD) is a well-known consequence of exposing an adsorbate-covered surface to a large photon flux via pulsed laser irradiation. Excited

electrons generated within the optical penetration depth of the surface decay rapidly (10⁻¹² s) by creation of phonons (thermal energy). The thermal energy diffuses away from the irradiated region both during and following cessation of the laser pulse. Depending upon the thermal diffusivity properties of the solid, it is possible to locally heat the surface at rates corresponding to more than 10¹¹ K/s.¹⁵

The temperature rise of a surface can be estimated using equation (1) when the optical and physical constants of the surface are known.¹⁶

$$\Delta T(t) = (F/K)(\kappa t/\pi)^{1/2} \tag{1}$$

Here, F is the energy absorbed by the surface, K is the thermal conductivity of graphite $(0.176 \text{ W/cmK})^{17}$, κ is the thermal diffusivity (0.56 cm/s) and t is the FWHM of the laser pulse (simplified to a triangular temporal profile). The energy absorbed, F, can be calculated from the optical penetration depth and the reflective properties of the surface. The optical penetration depth is given by $1/\alpha$, where α is the absorption coefficient for graphite. The absorption coefficients, calculated from the imaginary part of the refractive index of graphite, were $1.7 \times 10^5 \text{ cm}^{-1}$ at 193 nm, $3.6 \times 10^5 \text{ cm}^{-1}$ at 248 nm and $2.5 \times 10^5 \text{ cm}^{-1}$ at 351 nm. The Fresnel equations were used to determine the amount of energy absorbed and the amount of energy reflected from the surface.

The results of the calculation give an estimate of the change in surface temperature versus time and are shown in Figure 3.8 for a 193 nm, 16 ns FWHM laser pulse of 100 mJ/cm². The calculations for 248 nm and 351 nm light (not shown) were within 50 K of the data shown, largely because of the relatively uniform absorption coefficient of graphite over this wavelength range. At all three wavelengths, the surface temperature

rises well above the desorption temperature of butadiene, up to about 380 K in 16 ns from an initial sample temperature of 80 K. It should be noted that this isotropic model does not take into account the highly anisotropic thermal diffusivity (κ) of graphite. The value used (0.56 cm/s) is the quoted thermal diffusivity between the graphite sheets. Thermal diffusivity between the sheets is much slower and so our values for the transient temperature rises represent low estimates. Similarly, the use of the longest laser pulse FWHM in our calculations (16 ns) produces a low estimate of the maximum surface temperature rise.

To further investigate this process, the calculation was repeated for an incident power of 10 mJ/pulse (i.e. 10% of the original intensity). Under these conditions, it was found that the surface temperature increase is only about 30 K, or to about 110-115 K. This temperature increase corresponds to less than the temperature for onset of monolayer desorption for butadiene (about 120 K in TPD). In Figure 3.9 the amount of 1 ML desorbed from the surface was measured as pulse power was changed. The total number of photons striking the surface was constant for all the data shown and was $\sim 3 \times 10^{19}$ photons/cm². At low pulse power, ~0.064 W, the desorption was minimal and only about 5% of the monolayer was removed. At this power the maximum local surface temperature was calculated to be 121 K, close to the onset for desorption. At pulse powers above 0.1 W the amount of monolayer left on the surface greatly decreases. At these higher powers the surface temperature rise becomes significant. As a result, the desorption behavior of 1,3-butadiene adsorbed on graphite can be successfully described by a simple laser-induced thermal desorption mechanism. No other photochemistry was found to take place in the adsorbed monolayer or multilayer. This is surprising since

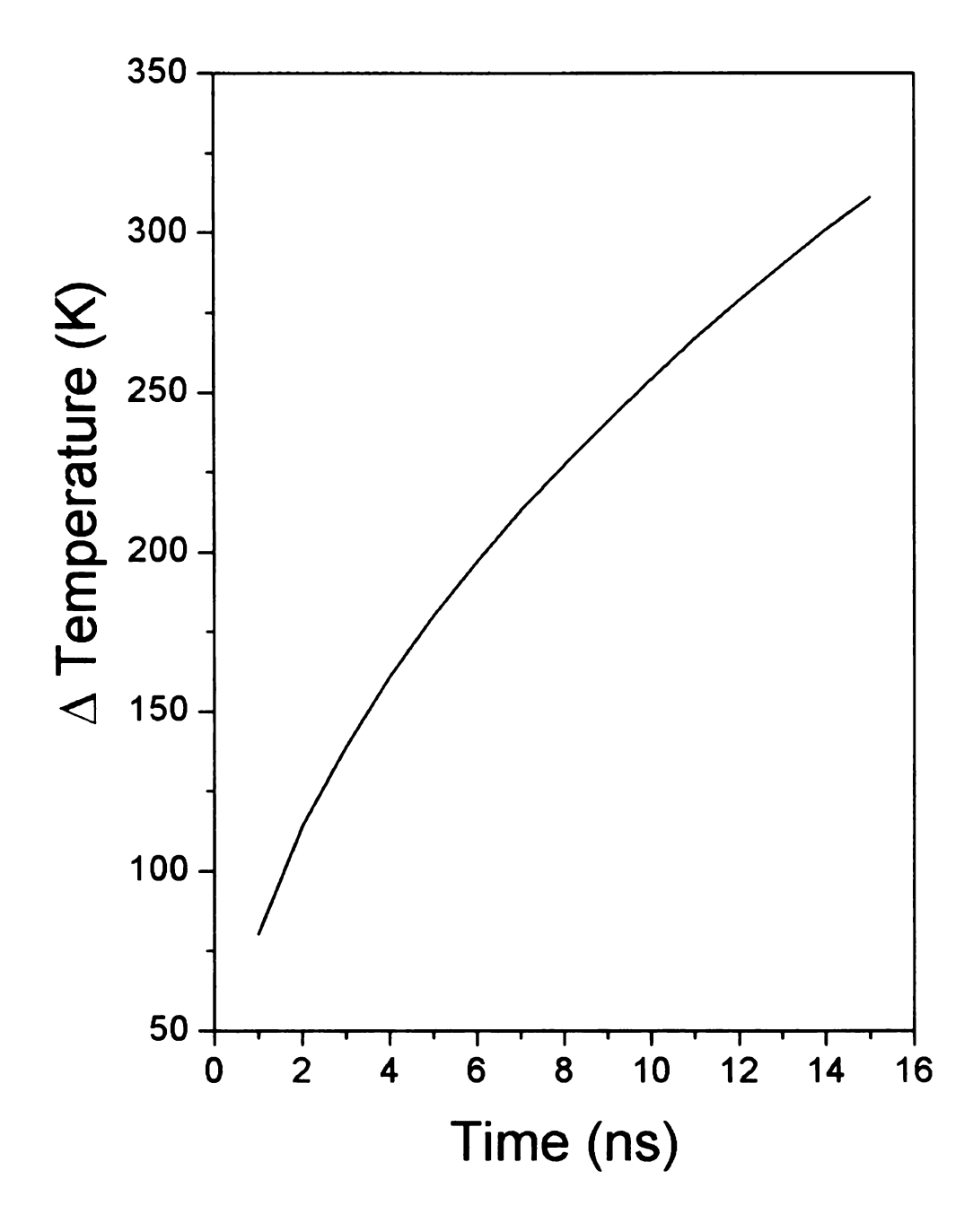


Figure 3.8 Result for calculating the surface temperature rise using equation 1 when HOPG is exposed to a 16 ns 100 mJ pulse of 193 nm light.

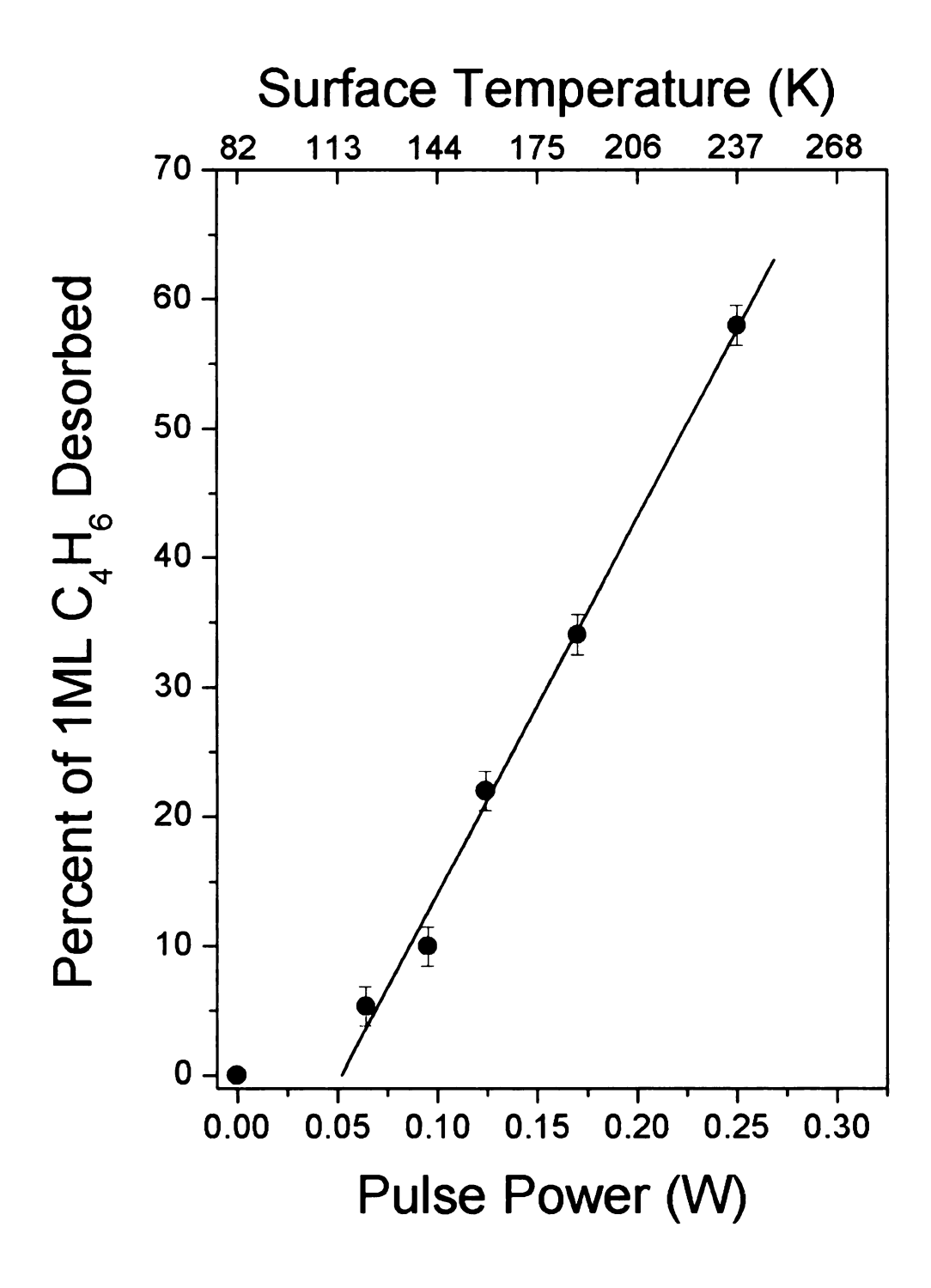


Figure 3.9 Percent of C_4H_6 monolayer desorbed from the surface with increasing pulse power. The total number of photons was kept constant at each pulse power by varying the number of pulses.

butadiene has been observed to polymerize from the gas-phase onto solid surfaces under UV light.²⁰ We speculate that the very short lifetime of the photoexcited state of adsorbed 1,3-butadiene (<100 fs for $C_4H_6(g)$), ¹³ prevents bimolecular reaction with neighboring species through diffusion in the monolayer.

3.9 Conclusions

The adsorption and photochemistry of butadiene (C_4H_6) on HOPG(0001) has been investigated. At < 85 K butadiene adsorbs on HOPG, probably forming 3-D islands on the surface as indicated by the appearance of multilayer TPD features before saturation of the first adsorbed layer. Temperature programmed desorption suggests that butadiene is physisorbed on the HOPG surface with a monolayer desorption energy of 32 kJ/mol. Electron energy loss spectroscopy suggests that the mirror axis of the molecule containing all atoms is parallel to the surface plane when adsorbed on HOPG, and that multilayers adsorb with the same geometry as the first layer.

Irradiation of both 1 and 3 ML coverages of C₄H₆/HOPG(0001) with high UV photon fluences (up to 100 mJ/pulse) over a range of wavelengths induces molecular photodesorption. Three possible desorption mechanisms were considered for the desorption process; (1) an adsorbate-mediated mechanism, (2) a substrate-mediated mechanism, and (3) a thermal mechanism. A simple thermal mechanism proved to offer the most reasonable explanation of the observed behavior, and calculations confirmed that at 100 mJ/pulse, the local surface temperature will rise to well above the desorption temperatures for butadiene. At lower energies (<10 mJ/pulse), no photodesorption or

other photochemistry was measured by TPD. Calculations suggest that the local surface temperature rise at these low energies is too small to thermally desorb butadiene from the monolayer.

3.10 References

- (1) Redhead, P. A. Vacuum 1962, 12, 203.
- (2) Jong, A. M.; Niemantsverdriet, J. M. Surf. Sci. 1990, 223, 355.
- (3) Shimanouchi, T. *Tables of Molecular Vibrational Frequencies*; NSRDS-NBS: 1972.
- (4) Mare, G. R. D.; Panchenko, Y. N.; Auwera, J. V. J. Phys. Chem. A 1997, 101, 3998.
- (5) Wiberg, K. B.; Rosenberg, R. E. J. Am. Chem. Soc. **1990**, 112, 1509.
- (6) Osaka, N.; Akita, M.; Itoh, K. J. Phys. Chem. B 1998, 102, 6817.
- (7) Weiss, M. J.; Hagedorn, C. J.; Weinberg, W. H. J. Vac. Sci. Technol. A **2000**, 18, 1443.
- (8) Zhou, X. L.; Zhu, X. Y.; White, J. M. Surf. Sci. Rep. 1991, 13, 73-220.
- (9) Ho, W. Surf. Sci. 1994, 299/300, 996.
- (10) Ho, W. J. Phys. Chem. 1996, 100, 13050.
- (11) Calvert, J. G.; Pitts Jr., J. N. *Photochemistry*; John Wiley and Sons: New York, 1966.
- (12) Fahr, A.; Nayak, A. K. Chem. Phys. 1994, 189, 725.
- (13) Fub, W.; Schmid, W. E.; Trushin, S. A. Chem. Phys. Lett. 2001, 342, 91.
- (14) Somorjai, G. A. *Introduction to Surface Chemistry and Catalysis*; John Wiley and Sons: New York, 1994.
- (15) Brand, J. L.; George, S. M. Surf. Sci. 1986, 167, 341.
- (16) Burgess, J.; Stair, P. C.; Weitz, E. J. Vac. Sci. Technol. A 1986, 4, 1362.

(17)

Воса

(18)

Pre

(19

Sa

(2

- (17) Lide, D. R., Ed CRC Handbook of Chemistry and Physics, 75th ed.; CRC Press: Boca Raton, FL, 1995.
- (18) Borghesi, A.; Guizzetti, G. *Handbook of Optical Constants of Solids 2*; Academic Press: 1991.
- (19) Ingle, J. D. J.; Crouch, S. R. *Spectrochemical Analysis*; Prentice-Hall: Upper Saddle River, New Jersey 1988.
- (20) Wright, A. N. Nature 1967, 215, 953.

CONCLUSIONS AND FUTURE WORK

4.1 Adsorption and Photochemistry of Butadiene on HOPG

The work presented in chapter 3 shows that butadiene adsorbs on HOPG at 85 K to form either mono or multilayer adsorption regimes depending on exposure. Temperature programmed desorption spectra indicate that butadiene desorbs molecularly from the HOPG surface at 105 K and 129 K for multi and monolayer coverages, respectively. The molecule adsorbs on HOPG with its mirror axis parallel to the plane of the surface in the *trans* conformation for all coverages as shown by EELS. Exposing the butadiene/HOPG surface to UV photons ($\lambda = 193$, 248, and 351nm) at high fluence (100 mJ/pulse) induces photodesorption of butadiene for both 1 and 3 monolayer coverages. Several well-known photodesorption mechanisms were considered including an adsorbate-induced process, a substrate-induced process and a laser-induced thermal desorption process. Based upon the wavelengths used, calculations for the surface temperature rise when exposed to high photon flux over a short period in time, and the reduced desorption of butadiene at lower pulse power (10 mJ/pulse) indicates that laser-induced thermal desorption is initiating the photodesorption of butadiene from HOPG.

An interesting finding of this work is that at low photon fluences, (\sim 10 mJ/pulse) where λ = 193, 248, and 351 nm, no condensed-phase photochemistry of butadiene on HOPG takes place. Photochemistry of butadiene in either the gas or liquid phase leads to the formation of a variety of products (see chapter 1). The lack of condensed phase

chemistry on HOPG may result from the ultra-short excited state life-time of butadiene, on the order of 100 fs.¹ Also, surfaces are known to shorten excited state life-times of adsorbates through a process called quenching.² Quenching processes are fast and have been know to compete with photo-driven chemistry of molecules adsorbed at metal interfaces.²

4.2 Future work

The fact that butadiene undergoes no photon-initiated chemistry in the condensed phase at low photon fluence leads to the possibility of investigating photon-initiated bimolecular reactions between butadiene and other photochemically active atmospherically relevant molecules, such as CH₃Br and NO₂, on the HOPG surface. To date, it is unclear what role the surface will play in reactions between butadiene and the photolysis products of CH₃Br and NO₂ in the condensed phase. The analytical techniques discussed previously including X-ray photoelectron spectroscopy, temperature programmed desorption and electron energy loss spectroscopy can be used to identify adsorbed state photochemical products, however, the adsorption structures and photochemistry of CH₃Br and NO₂, on HOPG must first be investigated.

Methyl bromide (CH₃Br) is prevalent in the atmosphere (10-15 ppt) and major sources include biomass combustion and biological activity in the ocean.³ The photochemistry of CH₃Br in the gas phase has been studied⁴ and absorption of UV radiation ($\lambda_{max} = 200 \text{ nm}$, $\sigma = 1 \times 10^{-18} \text{ cm}^2$) leads to $n \rightarrow \sigma^*$ from the Br atom to the C-Br antibonding orbital to form the photolysis products Br and CH₃. Free halogen atoms are known to add to unsaturated molecules across the double bond, and specific studies can

be found in the literature including reactions of chlorine atoms with butadiene and isoprene under atmospheric conditions.^{5,6}

Methyl bromide photochemistry has been studied on several different surfaces including metals^{2,7,8} and nonmetals^{9,10} under UHV conditions. On metal substrates the Br-C bond breaking occurs in the adsorbed state at photon wavelengths between 250 and 200 nm. Zhou and White⁸ investigated the photodissociation of CH₃Br on Ag(111) using XPS to determine changes in the chemical environment of the Br atom as a function of irradiation time. They measured the bromine 3d orbital binding energy in methyl bromide/Ag(111) to be 70.7 eV. Upon irradiation of the surface with a xenon arc lamp the two separate Br 3d peaks could be seen in the X-ray photoelectron spectra, one at 70.7 eV and the other at 68.7 eV. Further irradiation decreased the 70.7 eV peak area relative to the 68.7 eV peak area. The authors attribute the growth of the second peak at 68.7 eV to photodissociated Br atoms on the Ag(111) surface.

Some preliminary experiments to characterize the adsorption and photochemistry of CH₃Br on HOPG have already been preformed. Introduction of CH₃Br to the UHV chamber and HOPG surface was identical to that of butadiene as discussed in chapter 2. Figure 4.1 shows TPD data for the parent mass of the molecule, 94 amu, with increasing exposure times (1 sec to 60 sec) on the HOPG surface at 85 K. The broad background present in the TPD spectra, ranging from 100 K to 220 K, is attributed to desorption of CH₃Br from the molybdenum sample mount. The sharper peaks growing into the spectra at increased exposure are due to monolayer and multilayer desorption of CH₃Br from the HOPG surface at 115 K and 108 K respectively. Multilayer adsorption regimes begin to

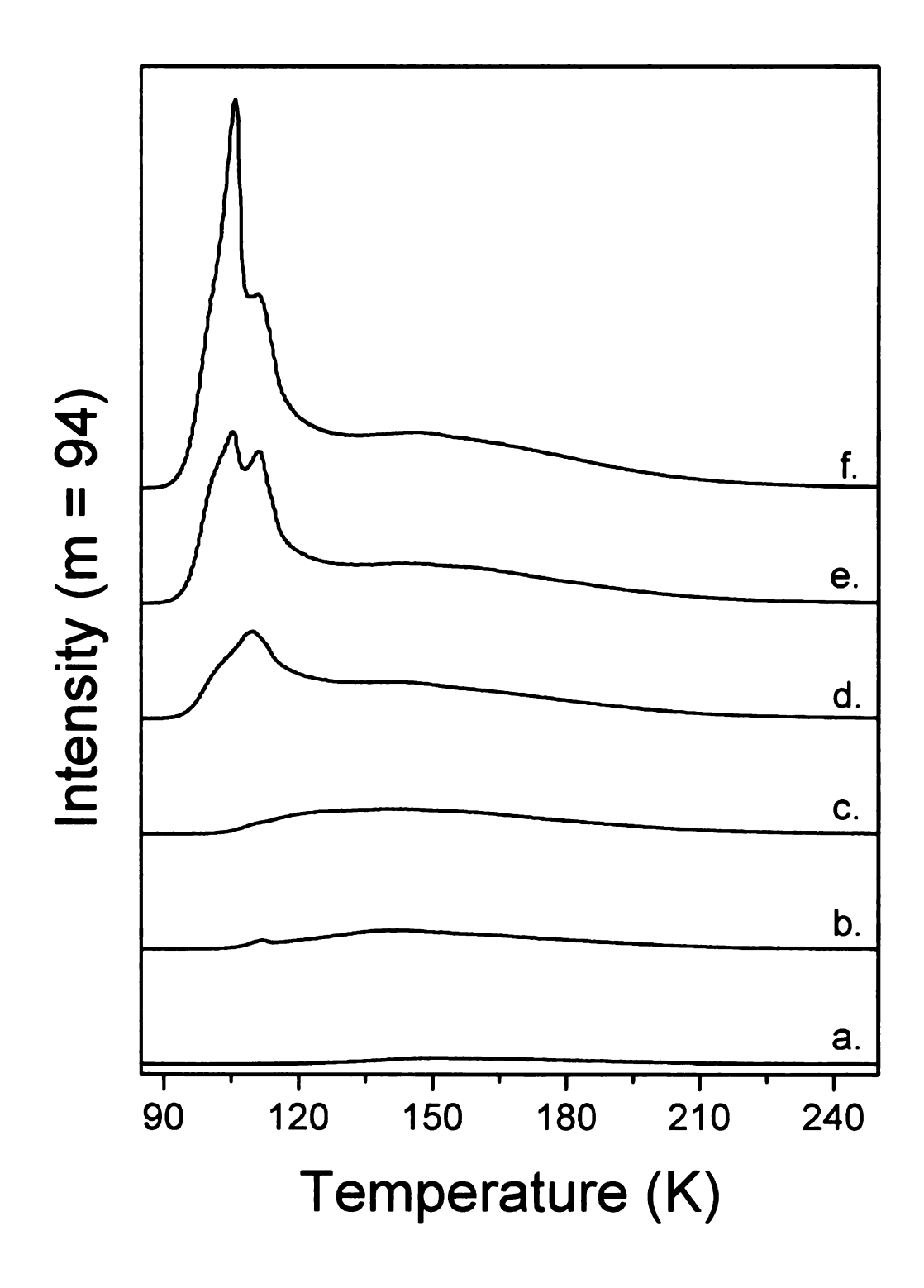


Figure 4.1 Temperature programmed desorption spectra (mass 94) for CH₃Br on HOPG with increasing exposure time; a) 1 sec, b) 5 sec, c) 10 sec, d) 20 sec, e) 40 sec, f) 60 sec.

form on the HOPG surface before the first monolayer is saturated as indicated by growth of the monolayer peak in the TPD spectra simultaneously with growth of the multilayer peak.

X-ray photoelectron spectroscopy was used to monitor the result of exposing 1 ML CH₃Br on HOPG to UV photons (λ = 193 nm) at low flux (~10 mJ/pulse). Figure 4.2 shows the Br (3d) XPS peak before and after various irradiation times. Before irradiation the binding energy was found to be 71.69 eV. After irradiation for 30 sec, two new peaks appeared in the X-ray photoelectron spectra, one at 70.92 eV and one at 68.48 eV. These two new peaks are attributed to surface bound Br atoms at 70.92 eV and possibly Br₂ at 68.48 eV, although further experiments will have to be performed to confirm this. Irradiation for longer time produces qualitatively similar results but an overall loss in XPS intensity indicates a decrease in total surface bound bromine. If either Br or Br₂ are formed on the surface as a result of irradiation, then either species could add to a double bond on butadiene.

Nitrogen dioxide (NO₂) is a photoactive molecule with similar release sources as both butadiene and carbonaceous aerosols. NO₂ photodissociates to form NO and O at wavelengths between 250 nm and 400 nm; the wavelength for maximum absorption is about 390 nm where the cross section is $6x10^{-19}cm^2.3$ NO₂ is known to play a significant role in the chemistry of both organics and ozone in the troposphere.³ In fact, oxidation reactions of organic molecules by various radicals in the presence of NO leads to the photodissociation of NO₂ in the troposphere. The adsorption of NO₂ has already been

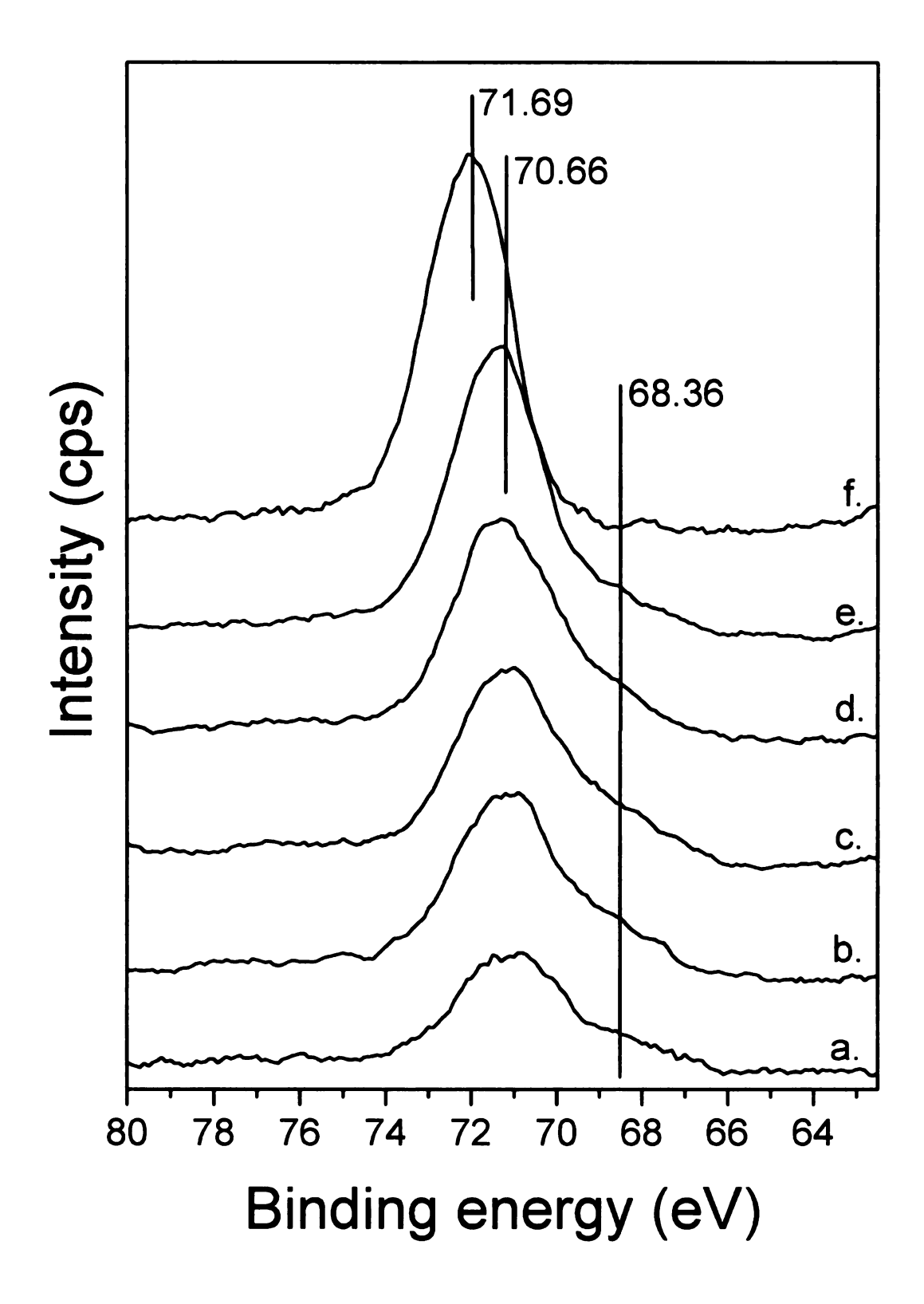


Figure 4.2 X-ray photoelectron spectra of 1 ML CH₃Br exposed to 5 mJ/pulses at 10 Hz of 193 nm light for increasing times; a) 30 min, b) 10 min, c) 5 min, d) 2.5 min, e) 0.5 min, f) 0 min showing binding energy changes.

studied on the HOPG surface by TPD and HREELS.¹¹ The molecule forms both mono and multilayers on graphite at 90 K which desorb at about 150 K and 140 K respectively. At all coverages, NO₂ reacts on the HOPG surface to form N₂O₄. Characterization of the condensed phase photochemistry of NO₂ on HOPG would have to be performed to determine if the products of the photochemical reaction, NO and O, remain adsorbed on the surface at 85 K.

In this thesis, a through study on the adsorption and photochemistry of butadiene on HOPG is presented, using HOPG as a model for carbonaceous aerosols. At high photon fluence (100 mJ/pulse) butadiene molecularly desorbs from the HOPG surface by way of a localized surface heating mechanism. At low photon fluences (10 mJ/pulse), butadiene shows no condensed phase photochemistry, even at wavelengths where the molecule has a large cross section for absorption. To further investigate any role carbonaceous aerosols may play in heterogeneous reactions in the atmosphere, further experiments need to be performed involving co-adsorbates with butadiene on the HOPG surface.

4.3 References

- (1) Fub, W.; Schmid, W. E.; Trushin, S. A. Chem. Phys. Lett. 2001, 342, 91.
- (2) Zhou, X. L.; Zhu, X. Y.; White, J. M. Surf. Sci. Rep. 1991, 13, 73-220.
- (3) Brasseur, G. P.; Orlando, J. J.; Tyndall, G. S. Atmospheric Chemistry and Global Change; Oxford University Press, Inc. New York, 1999.
- (4) Calvert, J. G.; Pitts Jr., J. N. *Photochemistry*; John Wiley and Sons: New York, 1966.
- (5) Ragains, M. L.; Finlayson-Pitts, B. J. J. Phys. Chem. A 1997, 101, 1509.
- (6) Wang, W.; Finlayson-Pitts, B. J. J. Geophys. Res. 2001, 106, 4939.
- (7) Lamont, C. L. A.; Conrad, H.; Bradshaw, A. M. Surf. Sci. 1993, 280, 79-90.
- (8) Zhou, X.-L.; White, J. M. Surf. Sci. 1991, 241, 259.
- (9) Heyd, D. V.; Jensen, E. T.; Polanyi, J. C. J. Chem. Phys. 1995, 103, 461.
- (10) Kim, S. H.; Stair, P. C.; Weitz, E. J. Chem. Phys. 1998, 108, 5080.
- (11) Sjovall, P.; So, S. K.; Kasemo, B.; Franchy, R.; Ho, W. Chem. Phys. Lett. 1990, 171, 125.

APPENDICES

Appendix A Mass Spectra

Before experiments, the gas phase cracking pattern of 1,3-butadiene was obtained to ensure purity. The molecule was introduced to the UHV chamber via the molecular leak valve. Mass spectra were collected from 0-50 amu for the background and 6-56 amu for butadiene, at 10 amu/sec. The electron multiplier voltage was set at 1.7 kV. The gas phase cracking pattern of butadiene collected with our mass spectrometer was compared with that reported by NIST. Qualitatively the spectra were identical expect for a mass 28 which is larger in our spectrum. The mass 28 signal is due to the oxidation of butadiene on the ion gauge filament to form carbon monoxide. This was tested by monitoring mass 28 signal with the ion filament on and off. During experiments the ion filament was kept on in order to monitor pressure in the chamber. Carbon monoxide does not stick to graphite at 77 K and so did not affect butadiene adsorption on HOPG during experiments.

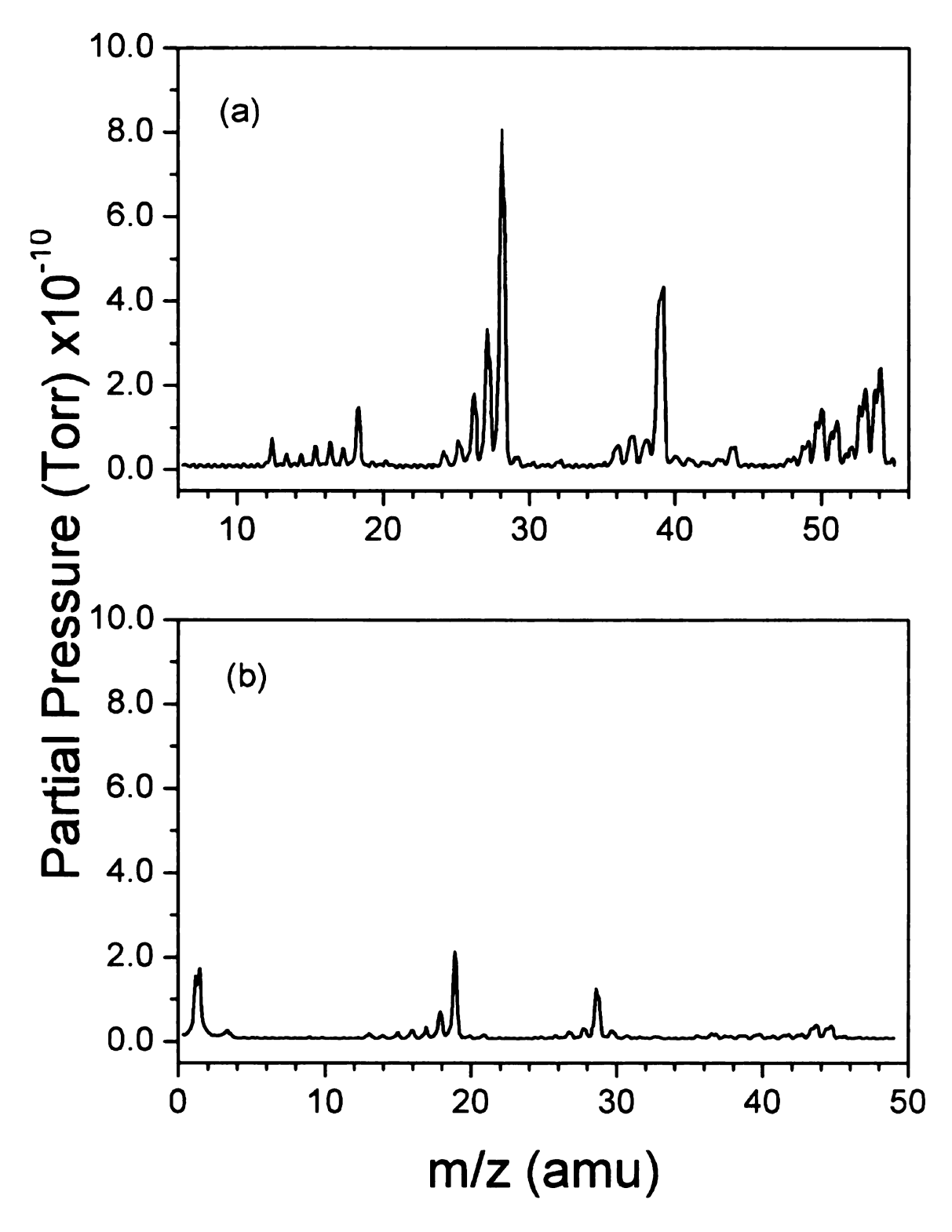


Figure A.1 Mass spectra of (a) 1,3-Butadiene at a pressure of $5x10^{-9}$ Torr and (b) the background vacuum of the chamber at a pressure of $2x10^{-10}$ Torr.

Appendix B Calculation of desorption energies for Butadiene on HOPG

The rate of desorption from a surface during a TPD experiment can be described using the Polanyi-Wigner equation.

$$-dn/dt = n^{x}v_{x} \exp(-E_{d}/RT)$$
 (1)

When desorption follows first-order kinetics the desorption energy can be determined using a modification of the Polanyi-Wigner equation developed by Redhead. In order to apply Redheads method E_d is assumed to be constant with both coverage and temperature. By setting x = 1, the temperature for the maximum rate of desorption can be determined by differentiating (1) to get:

$$dr/dT = r \cdot (E_d/RT_P^2 - v/\beta \exp(-E_d/RT_P))$$
 (2)

where β is the heating rate (K/s) and r the rate of desorption (dn/dt), then the temperature for maximum desorption occurs when.

$$E_d/RT_P^2 - v/\beta \exp(-E_d/RT_p) = 0$$
 (3)

Rearranging (3) gives

$$E_d = RT_P ((\ln(v_x T_P/\beta) - 3.46))$$
 (4)

where plots of E_d vs T_P produces a linear line when ν is between 10^{12} and 10^{14} Hz.

Multilayer desorption energies (zero order desorption processes) were determined by leading-edge analysis.² Equation (1) can be written as (take the ln of both sides)

$$\ln(-dn/dt) = \ln(\nu/\beta) - (E_d/R \cdot 1/T)$$
 (5)

Plots of $\ln(-dn/dt)$ vs 1/T gives a linear line where the slope is equal to (-Ed/R) and the intercept equal to $\ln(\nu/\beta)$. Both the frequency factor (ν) and E_d can then be determined by leading-edge analysis.

Appendix C Calculation for energy absorbed by

HOPG during laser irradiation

To determine the surface temperature rise of HOPG as a result of laser irradiation using equation 1 in chapter 3 the amount of energy absorbed by the surface must be calculated using the Fresnel equation for p polarized light.³

$$E_P = \frac{\cos\theta - \sqrt{(\eta_R^2 - \eta_I^2 - \sin^2\theta) + 1/(2\eta_R\eta_I)}}{\cos\theta + \sqrt{(\eta_R^2 - \eta_I^2 - \sin^2\theta) + 1/(2\eta_R\eta_I)}}$$

Where $(E_P)^2$ is the amount of energy reflected by the surface (R), η_R and η_I are the real and imaginary parts of the index of refraction for HOPG at 193 nm, 248 nm and 351 nm and are 1.67, 0.26, 1.51, 0.71, 2.02 and 0.69⁴ respectively and θ the angle of incidence. The complex quantity E_P can be reduced to a ratio of complex numbers.

$$R = (a^2 + b^2)/(c^2 + d^2)$$

Where the final result to calculate reflectivity at a incident angle is:

$$R = \frac{(\eta_R - 1/\cos\theta)^2 + \eta_I^2}{(\eta_R + 1/\cos\theta)^2 + \eta_I^2}$$

The reflectivity at wavelengths of 193 nm, 248 nm and 351 nm and an angle of incidence = 45° are calculated to be 1.3%, 5% and 6.8% respectively. Therefore the amount of energy absorbed by the surface is the total amount of energy exposed to the surface minus the percent reflected.

References

- (1) Redhead, P. A. Vacuum 1962, 12, 203.
- (2) Jong, A. M.; Niemantsverdriet, J. M. Surf. Sci. 1990, 223, 355.
- (3) Pedrotti, F. L.; Pedrotti, L. S. *Introduction to Optics*; Prentice Hall: Upper Saddle River, New Jersey, 1993
- (4) Borghesi, A.; Guizzetti, G. *Handbook of Optical Constants of Solids 2*; Academic Press: 1991

